ACS Catalysis

pubs.acs.org/acscatalysis

Perspective

Advances in the Molecular Catalysis of Dioxygen Reduction

Charles W. Machan*

Cite This: *ACS Catal.* 2020, 10, 2640−2655

Read Online

ACCESS | Metrics & More | Article Recommendations | Supporting Information

ABSTRACT: The reduction of dioxygen (O_2) is of vital importance to energy-related reactions. In biology, respiration uses O_2 reduction as a thermodynamic sink, whereas fuel cells pair the oxygen reduction reaction (ORR) to H_2O as a proton-dependent half-reaction to the oxidation of chemical fuels. Catalytic ORR processes mediated by molecular inorganic species continue to garner interest as models for heterogeneous systems. The ability to directly observe, quantify, and synthesize relevant intermediates from proposed reaction mechanisms renders molecular species readily optimizable, relative to the distribution of active sites within the nanoscale and mesoscale morphologies of heterogeneous systems. The development of next-generation cathode materials to displace platinum (Pt) for ORR will require improvements in the fundamental understanding of how O_2 behaves as a substrate, which well-defined homogeneous systems are uniquely positioned to provide. This Perspective provides a summary of recent advances in the area of homogeneous catalytic O_2 reduction, with a particular emphasis on improvements in activity and selectivity aided by mechanistic understanding.

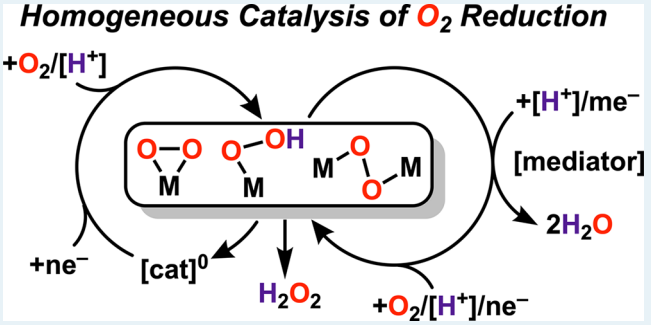

KEYWORDS: *dioxygen, catalysis, oxygen reduction reaction, homogeneous*

1. INTRODUCTION

Transition-metal compounds that can bind and activate dioxygen (O_2) are of continuing relevance to chemists interested in bioinorganic processes related to energy conversion, abiotic reactions relevant to solar fuels production, and aerobic oxidation chemistry.[1−14] These studies continue to necessitate an exploration of the fundamental properties of reactions using O_2 as a terminal oxidant, an area that has overlap with reactions involving the movement of protons and electrons, which can occur via asynchronous mechanisms or in concerted steps. As a result, a significant challenge to a rigorous understanding of observed O_2 reduction reactivity is the appropriate assignment of the relative importance of kinetic and thermodynamic parameters, as well as speciation, in controlling the primary reaction pathway. When transition-metal complexes with thermally accessible low- and high-spin manifolds are involved, the dominant reaction pathway can be difficult to deconvolute and changes in speciation can shift the identity of the resting state over the course of the reaction. Careful mechanistic study and critical evaluation of theoretical contributions can offer important insight into the behavior of these systems.

As a substrate, O_2 presents both experimental and conceptual pitfalls for accurate assessment of the dominant reaction pathway, because of its paramagnetic ground state. This can bias the analysis toward the role of spin state in the observed reactivity, although it is known that spin polarization effects can also result in viable reaction pathways.[15] For concerted proton−electron transfer reactions (CPET), whether the transferred electrons and protons arise from the same bond to form an analogous bond in the product or instead originate from distinct orbitals or spatial arrangements, the energetics of the bonds formed in the product molecule(s) relate to the barrier of the reaction, to some degree.[15] However, the connectivity between driving force and reactivity is a primary, but not the sole, determinant of concerted reactivity, and the geometry and spin-flexibility of transition-metal centers can alter the landscape of the free-energy surface in unexpected ways. Understanding relevant aspects of the electronic structure of key species, such as the lowest energy spin configuration of the products and spin polarization in the substrate, is a useful tool for explaining probable concerted pathways. Asynchronous pathways are often amenable to the assessment of the underlying thermodynamic parameters (standard potential and pK_a) that provide complementary understanding of the energetics of the concerted process.[16,17]

Once the double bond of O_2 is partially cleaved by one electron reduction (inner- or outer-sphere reduction pathways are possible), a variety of chemical transformations can occur: (1) the resultant superoxide can disproportionate into peroxide and O_2 or (2) direct reduction of superoxide into a peroxide or

Received: October 16, 2019
Revised: January 6, 2020
Published: February 7, 2020

https://dx.doi.org/10.1021/acscatal.9b04477
ACS Catal. 2020, 10, 2640−2655

water is possible. For the second pathway, bimetallic mechanisms can provide the necessary additional electron equivalents for direct reduction, as can an electrode or a chemical reducing agent.[7] The energetically favorable reduction of superoxide to H_2O_2 and $O_2^{2-}/HO_2^-/H_2O_2$ to water can also be used to drive paired electrochemical processes or oxidize small-molecule substrates.[7,18,19] This is the example set by nature, where Cytochrome *c* oxidases couple the reduction of O_2 to 2 equiv of water to provide a favorable energy gradient for ATP synthesis.[20−23]

Here, perspectives on recent reports on homogeneous electrocatalysts for O_2 reduction are presented. Readers interested in general surveys of molecular species capable of O_2 reduction, O_2 activation, catalytic aerobic processes, and the generation of high-valent species from O_2 are referred to other more exhaustive reviews and reports.[1−14,20−33] An additional related area of continuing interest beyond the scope of this Perspective is the use of immobilized molecular entities in heterogeneous catalyst systems.[34−36] Recent research focus in the area of molecular catalytic processes related to O_2 reduction has produced a series of paradigmatic changes with regard to how we view O_2-coupled reduction processes. This has resulted in the development of fundamentally new catalyst architectures, the optimization of previously known catalytic responses through thermochemical analyses, and a new understanding on the use of electron−proton mediators as co-catalysts. Following a brief summary of molecular catalytic O_2 chemistry, important recent advances will be described, concluding with a perspective on the field and future challenges.

2. A BRIEF HISTORICAL PERSPECTIVE ON THE CHEMISTRY OF DIOXYGEN AND TRANSITION METALS

Although the reversible binding of oxygen by cobalt salts was first reported by Fremy in 1852,[37] it was not until 1938 that Tsumaki proved that cobalt(II) Schiff base chelates could reversibly bind O_2 (the phenomenon was first observed in 1933 by Tsumaki and co-workers with the Fe derivative,[38] but not explained).[27,39] Concurrently with this, Pauling and Coryell conducted an experiment in 1936 which showed that a paramagnetic to diamagnetic transition occurs when deoxyhemoglobin reacts with molecular oxygen, which they concluded suggested a profound change in electronic structure had occurred.[40] Intense research continued during World War II, as interest in "on-demand" O_2 production drove the development of large-scale molecular carrier systems: Co(II)-salen (salen−*N*,*N*′-bis(salicylidene)ethylenediamine) was successfully used as the basis of a 350 ft^3/h O_2 generator for cutting and welding on a destroyer.[41] The unit served admirably on active duty in the Pacific Ocean until it failed when a crack developed in the head of its oxygen compressor from poor casting.[41]

Ongoing debates about the coordination mode of O_2 as a ligand in transition-metal complexes began to be answered later by X-ray techniques, with definitive structural evidence of O_2 binding by a Co(II) amine-based complex first reported in 1963.[42] The seminal achievement of Vaska to isolate an Ir complex with bound O_2 occurred that same year[43] (Vaska provided a crystal sample to Ibers and La Placa that was structurally characterized by X-ray methods in 1964[44]), which was rapidly followed by a wide array of synthetic oxygen carriers and mimics of natural systems.[28,31,32]

The desire to develop and isolate synthetic O_2-carrying molecules necessarily meant the concomitant development of design principles[29] which, when critically considered, also gave possible guidelines for the reduction of O_2 and development of oxidase mimics and catalysts for O_2 reduction.[20] For instance, within a hemoglobin metalloprotein, protons and Lewis bases are known to facilitate the loss of superoxide from the heme $[Fe(III)-O_2^{\bullet -}]$ adduct by protonation and ligand displacement reactions, respectively, creating reactive oxygen species. Synthetic oxygen carriers prevent analogous reactions through steric control in nonaqueous solutions, suggesting that bimetallic active sites or deliberate inclusion of a suitable base or a proton source could accelerate reduction in an ORR catalyst.[20,28,29]

However, this type of "reverse engineering" does not always follow a straight path to improved catalyst activity: although the protonation of a metal-bound superoxide species can be rate-limiting in molecular catalytic systems,[45] the inclusion of pendent proton sources in the ligand framework do not necessarily optimize the catalytic response by enhancing the rate of $[M-O_2^{\bullet -}]$ protonation. Although some apparent indirect correlations can be observed,[46] the difference in activity of these modified catalyst constructs is often better rationalized as the result of the tuning of formal catalyst potentials[47,48] or reaction medium effects.[49] Where this strategy has been successful, however, is in cases where O−O bond cleavage of a hydroperoxo intermediate to generate water is rate-limiting in the probable mechanism.[50−52] At catalytic potentials where both H_2O_2 and H_2O are thermodynamically viable products, the use of multimetallic active sites can be used to alter kinetic selectivity by increasing the number of available reducing equivalents and altering the reaction pathway to include multipoint activation.[53−56] Recent studies have also shown that the inclusion of redox-active active small-molecule electron−proton mediators[57,58] can improve the catalytic response by acting to reduce intermediate superoxide species through concerted and asynchronous transfer of proton and electron equivalents. Continuing interest in efficient chemical oxidations and fuel cell technologies supports ongoing efforts in the study of molecular catalysts for the reduction of O_2. Increasingly interdisciplinary approaches are recognizing overlaps with related research areas, resulting in new fundamental understanding of O_2 as a substrate in catalytic reactions.

3. MOLECULAR ORBITAL STRUCTURE OF DIOXYGEN, FUNCTION AS A LIGAND, AND REDUCTION

O_2 is commonly used as an illustrative example of the limitations of the Lewis dot structures in introductory chemistry courses, because it fails to adequately explain the paramagnetism observed experimentally.[59] The paramagnetic triplet ground state of O_2 is readily understood with a simple molecular orbital diagram (Figure 1). Consistent with its properties as a ligand, orbital vacancies accommodate electron density as a π-acid, specifically in degenerate antibonding orbitals. The π-acid properties are significant enough that, in most cases, O_2 binding occurs with formal reduction of the oxygen−oxygen bond to produce a bound superoxide (or peroxide), although there are exceptions.[60−63] Unimolecular O_2 binding and activation can result in η^1- and η^2-superoxide complexes,[64] from which protonation or ligand substitution reactions cause the displacement of superoxide or related species.[20,28,29] Synthetic O_2 carriers have used elaborate coordination motifs to protect the site of O_2 binding, emulating the function of large hydrophobic

https://dx.doi.org/10.1021/acscatal.9b04477
ACS Catal. 2020, 10, 2640−2655

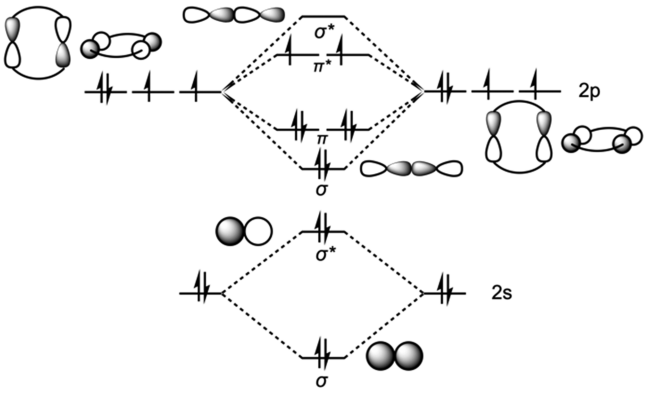

Figure 1. Molecular orbital energy diagram of O_2.

regions in the heme proteins.[20,28,29] Bimetallic coordination motifs also exist with comparable "end-on" or "side-on" binding modes.[64]

The binding mode and covalency of the M−O_2 interaction is highly dependent on *d* electron count of the metal center involved when formal reduction from $^3O_2$ to $^2O_2^{\bullet-}$ occurs (note that the preceding superscript used here corresponds to 2S + 1). As a qualitative comparison, ground-state structures for Co and Fe [M(*meso*-tetraphenylporphyrin)(η^1-$O_2^{\bullet-}$)(1-methylimidazole)]^0 adducts, [M(TPP)(η^1-$O_2^{\bullet-}$)(1-MeIm)]^0, which both favor the "end-on" binding mode, have been calculated using unrestricted DFT methods and analyzed through quasi-restricted orbital plots.[65−67] In both cases, these qualitative electronic structure calculations are consistent with previous proposals that the formally M(II) centers are oxidized to a formally low-spin M(III) state upon O_2 binding: either doublet Fe, ^{2}Fe(III), or singlet Co, ^{1}Co(III) (see Figures 2 and 3).[68−72]

For the ^{2}Fe(III) fragment, with a putative d^5 electron configuration in a pseudo-octahedral environment, there is partial population of a set of *d* orbitals that can be π-symmetric, with respect to the end-on $^2O_2^{\bullet-}$ ligand. Assessing the bonding interaction for the antiferromagnetically coupled ^{2}Fe(III)−$^2O_2^{\bullet-}$ core suggests that a key component of the diamagnetic ground state is a π-bonding interaction between the partially occupied perpendicular π^* manifold of $^2O_2^{\bullet-}$ and this *d* orbital set (Figure 2D). Here, perpendicular and parallel are descriptors meant to indicate the approximate orientation of the orbital, with respect to the vector described by the Fe−O bond. This interaction strengthens the Fe−O bond (which contains an additional σ donor−acceptor interaction between a now fully occupied parallel π^* antibonding orbital and the Fe center; see Figure 2C) and slightly weakens the O−O bond relative to the Co-based analogue, vide infra. The LUMO of the diamagnetic ground state is predicted to comprise the remaining π^* orbital vacancy in superoxide, which is antibonding with respect to the vacancy in the π-symmetric *d* orbital (Figure 2B).

In [Co(TPP)(η^1-$O_2^{\bullet-}$)(1-MeIm)]^0, the interaction between low-spin ^{1}Co(III) and $^2O_2^{\bullet-}$ is much weaker due to the absence of a π-bonding interaction into the partially occupied perpendicular π^* antibonding orbital set of $^2O_2^{\bullet-}$. In the SOMO orbital projection (Figure 3B), the $^2O_2^{\bullet-}$ fragment does not form a substantial interaction with the π-symmetric *d* orbitals (Figure 3D), in contrast to the distribution between the ^{2}Fe(III) and $^2O_2^{\bullet-}$ fragments predicted for the lowest energy orbital vacancy in the Fe system (Figure 2B). The primary bonding interaction is of σ donor−acceptor character between the fully occupied parallel π^* antibonding orbital of superoxide

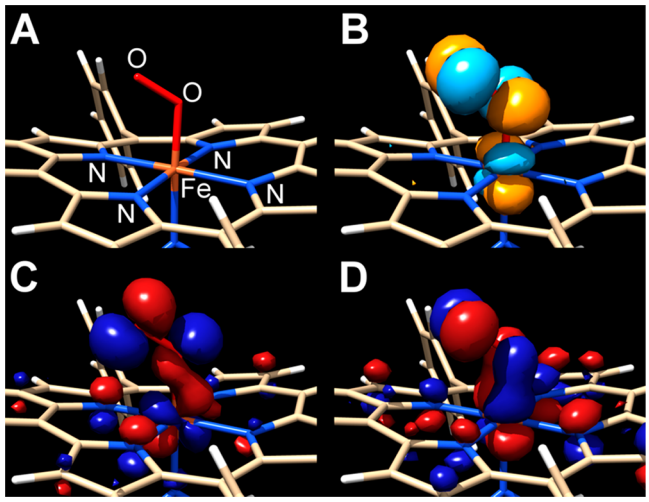

Figure 2. Selected quasi-restricted orbitals of [Fe(TPP)(η^1-$O_2^{\bullet-}$)(1-MeIm)]^0 highlighting (A) the primary bonding interactions between the superoxide fragment and the Fe metal center; (B) unoccupied −3.45 eV; (C) doubly occupied −6.10 eV; and (D) doubly occupied −6.19 eV. DFT calculations performed using ORCA 4.2.1:[73] B3LYP/G[74−78] functional, def2-SVP[79,80] basis set, RIJCOSX approximation,[81] D3BJ dispersion correction,[82,83] and CPCM[84] to model the DMF solvent.

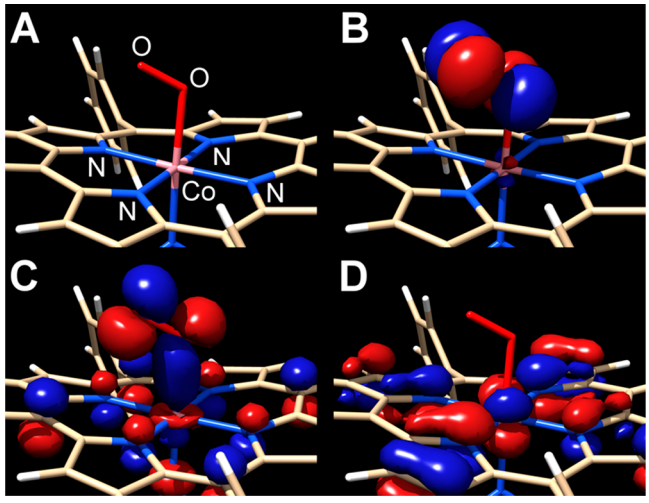

Figure 3. Selected quasi-restricted orbitals of [Co(TPP)(η^1-$O_2^{\bullet-}$)(1-MeIm)]^0 highlighting the primary bonding interactions between (A) the superoxide fragment and the Co metal center; (B) singly occupied −4.53 eV; (C) doubly occupied −4.94 eV; and (D) doubly occupied −6.46 eV. DFT calculations performed using ORCA 4.2.1:[73] B3LYP/G[74−78] functional, def2-SVP[79,80] basis set, RIJCOSX approximation,[81] D3BJ dispersion correction,[82,83] and CPCM[84] to model the DMF solvent.

and the Co center (Figure 3C). This results in an elongated Co−O distance of 2.104 Å, compared to an Fe−O distance of 1.753 Å.[65] The additional π-symmetric bonding interaction in [Fe(TPP)(η^1-$O_2^{\bullet-}$)(1-MeIm)]^0 results in only minor differences in O−O distance (1.265 Å for the Fe), with respect to [Co(TPP)(η^1-$O_2^{\bullet-}$)(1-MeIm)]^0 (1.249 Å for the Co), suggesting a high degree of localization in the Fe−O interaction.[65] For comparison, $^3O_2$ has an estimated bond distance of 1.204 Å at this level of theory.

Our discussions of reported catalytic behavior below note that, in comparing the two, [Fe(TPP)]$^+$-based catalysts are

https://dx.doi.org/10.1021/acscatal.9b04477
ACS Catal. 2020, 10, 2640−2655

generally selective for H_2O, while Co analogues can produce mixtures of H_2O and H_2O_2, if thermodynamic reaction parameters are not carefully controlled. From a qualitative analysis of charge distribution, the metal-bound oxygen atom is relatively more negative for the ^{1}Co(III)−$^2O_2^{\bullet-}$ species than the ^{2}Fe(III), see the Supporting Information, consistent with the possibility of competitive protonation to produce mixtures of H_2O_2 and H_2O. The comparative thermodynamic accessibility of an Fe(IV) oxo species from O−O bond cleavage, with respect to the comparable Co(IV) oxo in a pseudo-octahedral environment, is also expected to contribute to a difference in selectivity for H_2O as the reduction product.[85]

The case of the binding and activation of O_2 by a comparable Mn(II) porphyrin species does not readily lead to comparison with the Fe and Co examples.[68,86] Phung and Pierloot have calculated that Mn prefers to bind O_2 in a side-on fashion without a *trans* ligand, in a quartet ground-state that contains a minor ^{3}Mn(III)-$^2O_2^{\bullet-}$ component and a major ^{4}Mn(IV)-$^1O_2^{2-}$ component.[86] These predictions, which compare well with experimental data, describe a degree of activation between $^2O_2^{\bullet-}$ and $^1O_2^{2-}$, which is greater than that achieved in the "end-on" six-coordinate Fe- and Co-based model systems discussed above. Consistent with the hypothesis that greater initial O_2 activation is occurring in Mn(porphyrin)-based complexes, recent results suggest that H_2O is the primary product in nonaqueous conditions with an added proton donor[51] and in buffered aqueous systems,[87] although end-on coordination modes are thought to be likely intermediates following further reduction and protonation.[51]

4. RECENT ADVANCES IN O_2 REDUCTION

4.1. The (Complete) Mechanism of ORR by [Fe(TPP)]$^+$. A recent comprehensive study by Pegis et al. detailed all the relevant equilibria, kinetic and thermodynamic parameters of ORR by [Fe(TPP)]$^+$ under catalytic conditions with tosic acid (TsOH) as a proton donor.[45] Although many of the results were consistent with mechanistic proposals and prior work,[4,7,47,88,89] the complete mechanistic model incorporating experimental and computational studies was independently supported by multistate kinetic modeling *under a single set of conditions for the first time*. Interestingly, the multistate modeling of the overall reaction predicts a shifting of the resting state of the catalytic cycle as the reaction proceeds and relative substrate concentrations begin to shift. Scheme 1 highlights the features of the overall proposed catalytic ORR reaction mechanism: reduction of the resting state, [Fe^{III}(TPP)]$^+$, generates [Fe^{II}(TPP)]^0, which binds O_2 reversibly to form the superoxide species, [Fe^{III}(TPP)($O_2^{\bullet-}$)]^0. The rate-determining step in the ORR mediated by [Fe(TPP)]$^+$, in this case, is the protonation of [Fe^{III}(TPP)($O_2^{\bullet-}$)]^0 by TsOH, which has an experimentally determined kinetic barrier of ∼11 kcal/mol. Subsequent reduction and protonation steps of the protonated superoxide rapidly generate water under these conditions. Computational modeling suggests that the overall barrier contains contributions from both the equilibrium preassociation of the proton donor to the Fe-bound superoxide *and* the kinetic rate of formal proton transfer from within the resultant noncovalent adduct, once appreciable desolvation of the proton donor has occurred.[45] In this study, the experimental results showed excellent correlation between spectrochemical (where decamethylferrocene (Cp^*_2Fe) is used as a reductant) and electrochemical measurements (where reducing equivalents are supplied by a potentiostat), an agreement that has been demonstrated for the [Fe(TPP)]$^+$ system previously.[47,88] The level of detail in the experimental rigor of this approach is exemplified by the ability to independently compare mechanistic details between distinct experimental techniques. We note that incompatibilities between the required reaction conditions to appropriately compare spectrochemical and electrochemical measurements can result in unanticipated mechanistic changes, vide infra, which obviate the ability to use this direct experimental comparison approach for all catalyst systems.

Scheme 1. Proposed Mechanism for Oxygen Reduction Catalyzed by [Fe^{III}(TPP)]$^+$, with TPP Abbreviated as an Oval[a,b]

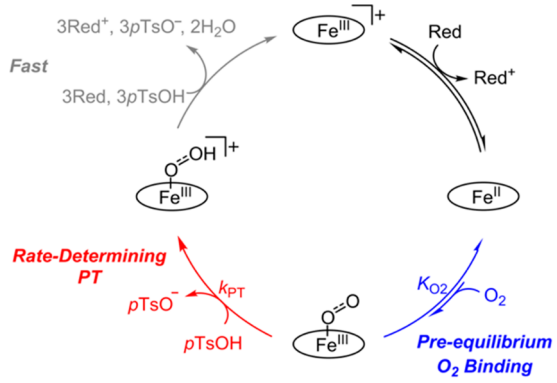

[a]Red = Cp^*_2Fe or electrode. [b]Reprinted with permission from ref 45. Copyright 2019, American Chemical Society, Washington, DC.

4.2. Recent Progress in Mn ORR Catalysts. Inspired by a relative lack of reports on Mn ORR catalysts, in comparison to Fe and Co systems, our group undertook a series of mechanistic investigations on a Mn-based catalyst, Mn(^{tbu}dhbpy)Cl, where [^{tbu}dhbpy]$^{2-}$ = 6,6′-di(3,5-di-*tert*-butyl-2-phenolate)-2,2′-bipyridine (Figure 4).[90,91] Under electrocatalytic conditions with 2,2,2-trifluoroethanol (TFE) as a proton donor, the system generates H_2O_2 with ca. 80% Faradaic efficiency, as determined through rotating ring-disk electrode measurements (Figure 4).[90]

This system exhibits a significant pre-equilibrium effect on catalyst redox potential, with added proton donors (both buffered and unbuffered) inducing a shift in the observed Mn(III)/(II) reduction potential toward more-positive potentials (see Figure 5A). Through an electrochemical analysis of the mechanism responsible for this shift in potential, including a study on the use of proton donors with varied pK_a (acetonitrile (MeCN)), we were able to establish that a Nernstian 1e$^-$/1H$^+$ process was occurring. Part of this analysis included assembling a potential-pK_a diagram in MeCN (Figure 5B);[90] potential-pK_a diagrams compare acids at low concentrations to mitigate the deleterious effects of homoconjugation,[92] enabling a Pourbaix-type analysis in nonaqueous systems without needing to describe a solvated proton concentration.[93] We have proposed that this Nernstian process corresponds to a multisite reaction, where reduction of the Mn(III) center results in a corresponding protonation of a Mn-bound O atom on the ligand framework. This reaction is noteworthy because the distribution of the added 1e$^-$/1H$^+$ between the metal center and the ligand framework results in the retention of a vacant coordination site for O_2 binding, "preloading" the catalyst to bind and activate O_2. In addition, the expected dependence of the protonated O atom's acidity on the Mn oxidation state suggests that O_2 binding and reduction will control proton transfer from the ligand to the substrate during catalytic reduction. Indeed, under

https://dx.doi.org/10.1021/acscatal.9b04477
ACS Catal. 2020, 10, 2640−2655

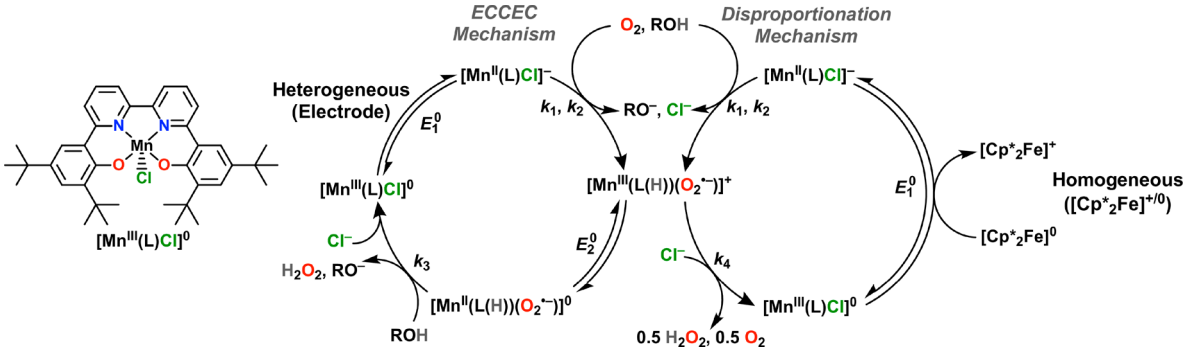

Figure 4. Proposed complete catalytic cycles for O_2 reduction driven by the electrode (heterogeneous) and driven by Cp^*_2Fe (homogeneous); L = ^{tbu}dhbpy^{2-}, ROH = a generic proton donor, and [Mn^{III}(L)Cl]^0 = Mn(^{tbu}dhbpy)Cl. [Adapted with permission from ref 91. Copyright 2019, American Chemical Society, Washington, DC.]

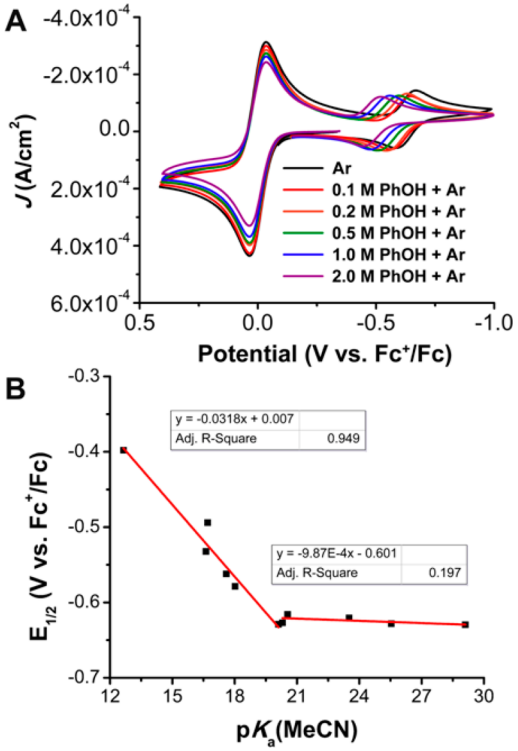

Figure 5. (A) Cyclic voltammograms of Mn(^{tbu}dhbpy)Cl, obtained under argon saturation conditions with variable PhOH concentration, demonstrating the Nernstian shift of the Mn(III)/(II) reduction feature as a result of a pre-equilibrium involving the added proton donor and the inorganic complex. (B) A potential−pK_a diagram for acids from pK_a(MeCN) 12.65 to 29.14. [Adapted with permission from ref 90. Copyright 2017, American Chemical Society, Washington, DC.]

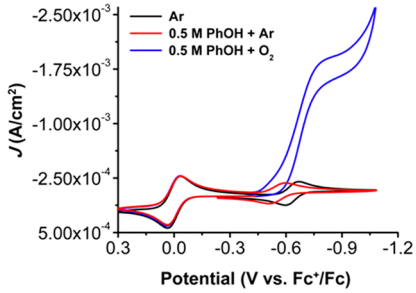

Figure 6. Cyclic voltammograms of Mn(^{tbu}dhbpy)Cl, obtained under argon saturation conditions (black), argon saturation with 0.5 M added PhOH demonstrating a Nernstian shift in formal redox potential (red), and O_2 saturation with 0.5 M added PhOH demonstrating a catalytic response at potentials reflecting the pre-equilibrium redox shift (blue). [Adapted with permission from ref 90. Copyright 2017, American Chemical Society, Washington, DC.]

O_2 saturation conditions with either phenol (PhOH; see Figure 6) or TFE present as a sacrificial proton donor, an electrocatalytic response is observed that is shifted from the formal Mn(III)/(II) potential observed under aprotic conditions. Variable concentration studies on the relationship of the observed catalytic current response to the amount of added catalyst, O_2, and proton donor showed a first-order dependence for each, consistent with the reduction and protonation of an intermediate Mn(II) superoxide as the rate-determining step (left cycle; see Figure 4).[90]

Inspired by the work of Mayer and co-workers to establish a correlation between spectrochemical and electrochemical experiments in the analysis of the catalytic ORR,[45,47,88] we explored the mechanism of Mn(^{tbu}dhbpy)Cl in greater detail in a subsequent publication.[91] Using stopped-flow rapid-mixing spectrochemical experiments with Cp^*_2Fe as a chemical reductant, we attempted to correlate the catalytic response of a series of buffered proton donors to compare with electrochemical experiments. Unexpectedly, while the electrocatalytic response was pK_a-dependent and activity conformed strictly to the reported standard potential,[7] analogous pK_a dependence was not observed under spectrochemical conditions, although H_2O_2 was still detected.

Additional thermochemical analyses, as well as systematic testing, revealed that a mechanism shift occurs under spectrochemical conditions with Cp^*_2Fe as a homogeneous reductant, where a disproportionation reaction involving the intermediate Mn(III) superoxide species alters the overall reaction to thermodynamically allow H_2O_2 production under conditions that are counterthermodynamic for electrocatalysis (right cycle, Figure 4). The nearly S-shaped electrocatalytic wave that we observed with both nonbuffered[90] and buffered[91] proton donors suggests that the kinetic limitations of the catalyst impose conditions where the reaction-diffusion layer is deficient in active catalyst, relative to the availability of substrate.[94] Conversely, spectrochemical conditions are chosen so that they can be limited by the amount of available O_2 substrate, such that direct comparisons with electrocatalytic conditions can be made in common terms of O_2 consumption.[45,47,88] Furthermore, additional control experiments showed that the reduction of the intermediate Mn(III) superoxide species requires more negative

https://dx.doi.org/10.1021/acscatal.9b04477
ACS Catal. 2020, 10, 2640−2655

potentials (E_2^0) than the initial reduction (E_1^0) (recall Figure 4). This is trivial to satisfy during a cyclic voltammetry (CV) experiment at moderate scan rates, because of the modest turnover frequency of this catalyst, but the use of a solubilized chemical reductant relies on relatively fixed reducing power, meaning that the multistep reduction reaction becomes more difficult from E_1^0 to E_2^0. As a result, while a pK_a-dependent electrocatalytic response is observed, under spectrochemical conditions, H_2O_2 is still generated with acids too weak to do so under electrochemical conditions via a disproportionation pathway as the intermediate Mn(III) superoxide species accumulates. We note that, from a speciation perspective, however, the likelihood of the disproportionation of 2 equiv of the Mn(III) superoxide intermediate should decrease over time as the limiting O_2 concentration begins to restrict its formation. We speculate that, with the increasing depletion of O_2 as the reaction proceeds, either (i) Mn(II) species can mediate disproportionation of the Mn(III) superoxide to H_2O_2 or (ii) a redox equilibrium between the Mn(III) superoxide and $[Cp^*_2Fe]^+$ is established, both of which will be considered in future studies on speciation over time.

These studies with Mn(^{tbu}dhbpy)Cl have shown how the catalytic response can be tuned through pre-equilibrium reactions between the proton donor and the catalyst, without occupying a metal coordination site, to create an activated intermediate species. In addition, we have shown that comparing catalytic behavior through the use of counterthermodynamic conditions can be useful in isolating changes in mechanism. The difference in required reaction conditions to compare spectrochemical and electrochemical data can cause changes to the overall reaction that would be difficult to identify without the experimental tools enabled by thermochemical analysis.

Following our study, Nocera and co-workers reported a series of Mn porphyrins for ORR in MeCN, wherein a combination of rigorous experimental testing and CV modeling were able to establish the limiting steps of the overall mechanism for the catalyst structures with and without a pendent functional group present (see Figure 7).[51] The pendent functional groups

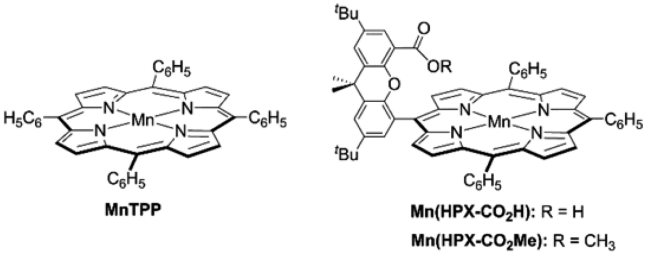

Figure 7. Manganese(II) tetraphenylporphyrin (MnTPP) and hangman porphyrin xanthene compounds (Mn(HPX-CO_2H) and Mn(HPX-CO_2Me)) that electrocatalyze O_2 reduction to H_2O in acetonitrile. [Reprinted with permission from ref 51. Copyright 2018, American Chemical Society, Washington, DC.]

included a comparison between the inclusion of a relatively acidic proton and its corresponding ester to isolate the effect on the catalytic response.

Mechanistic experiments and thermochemical analyses established that the mechanism proceeds via an initial Mn(III)/(II) reduction, followed by an O_2 binding step to generate a pre-equilibrium complex. The initial O_2 adduct (both resonance forms) and the end-on Mn(III) hydroperoxide generated by subsequent one-electron reduction and proto-

nation are stabilized by hydrogen-bonding interactions with 2 equiv of the sacrificial proton donors. These noncovalent interactions result in an overall second-order concentration dependence, with respect to the catalytic response in all cases for the unadorned MnTPP and at high concentrations of added acid for the pendent-functionalized Mn(HPX-CO_2H) (see Figure 7). Conversely, at low acid concentrations, pendent hydrogen bonding interactions from the carboxylic acid in Mn(HPX-CO_2H) can assist in the stabilization of the initial O_2 adduct, resulting in first-order concentration dependence on added acid. The rate-determining step of the catalytic cycle is the cleavage of the O−O bond in the hydroperoxo intermediate (see Scheme 2). Indeed, all observed concentration dependences and CV

Scheme 2. Overall Mechanism of ORR by Mn Porphyrin Derivatives[a]

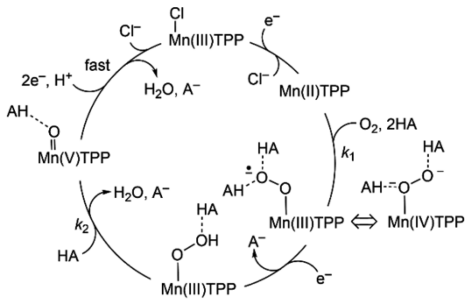

[a][Reprinted with permission from ref 51. Copyright 2018, American Chemical Society, Washington, DC.]

modeling established that the O_2 binding step and subsequent reduction and protonation to the bound hydroperoxide were generally much more rapid than the final O−O bond cleavage step. Brønsted plots for both of these reaction steps had negative slopes, consistent with large reaction driving forces: (1) in the case of hydroperoxo formation, an irreversible step follows an early transition state, with 2 equiv of acid facilitating an electron transfer step that is not rate-determining; (2) the shallow slope of the O−O bond cleavage step suggests that the acid is an active chemical promoter for the rate-determining step. The hangman construct can be well-suited for improving catalytic performance; however, in this case, the benefit is rapidly overwhelmed at high acid concentrations, minimizing its relative contribution.

This study noted that there is CV evidence of an off-cycle intermediate under aprotic conditions when O_2 is present, which the authors suggested could be analogous to the side-on (super)peroxide adduct discussed in Section 3. Other reports under aprotic conditions,[95−97] frozen in Ar matrixes,[98] and the computational methods described above,[86] have characterized and proposed a similar side-on binding mode of dioxygen to a Mn(II) porphyrin. The experimental results of Nocera and co-workers are consistent with the binding and two-electron reduction of O_2 being rapid and resulting in the formation of an end-on hydroperoxide species, suggesting that the presence of acid under reducing conditions flattens the free-energy surface between the end-on and side-on binding modes of O_2. It is probable, however, that the "off-cycle" side-on mode is relevant to the high affinity of Mn(II) porphyrin for oxygen, relative to its Fe(II) equivalent.[86,98]

4.3. Thermochemical Reaction Control for O_2/H_2O_2.

Stahl and co-workers[99] recently described a catalyst system where reaction product control could be selectively achieved through thermodynamic bracketing (Figure 8). Disappointingly,

https://dx.doi.org/10.1021/acscatal.9b04477
ACS Catal. 2020, 10, 2640−2655

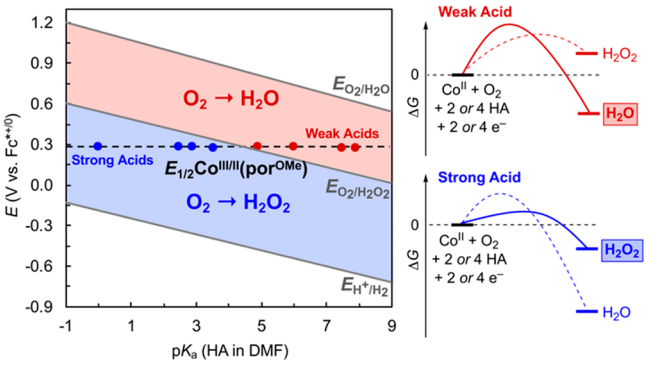

Figure 8. Table correlating the pK_a(DMF) of acids with the H^+/H_2 and O_2/H_2O_2 standard potentials. While the proton-dependent O_2/H_2O_2 standard potentials shift with a Nernstian dependence on acid strength, the $E_{1/2}(Co^{III/II})$ reduction potential of Co(por^{OMe}) (por^{OMe} = meso-tetra(4-methoxyphenyl)porphyrin) is independent of the acid pK_a. As a result, thermodynamic bracketing of the reaction product occurs, with weak acids almost exclusively favoring the $4e^-/4H^+$ reduction of O_2 to H_2O, while strong acids predominantly favor the $2e^-/2H^+$ reduction of O_2 to H_2O_2. [Reprinted with permission from ref 99. Copyright 2019, American Chemical Society, Washington, DC.]

in our Mn-based system, moving to counterthermodynamic conditions for electrocatalytic ORR to H_2O_2 did not alter product selectivity to H_2O; instead, no electrocatalytic activity was observed.[91] Analogous knowledge of the standard potentials under nonaqueous conditions allowed Stahl and co-workers to completely shift product selectivity between H_2O_2 and H_2O by tuning reaction standard potentials while maintaining high current efficiency using Brønsted acid scaling relationships.[99] The driving hypothesis was focused on the notion that there is an intuitively simpler way to tune reaction selectivity than trying to develop kinetically selective catalysts: use reaction thermodynamic parameters to exclude the possibility of forming specific reaction products. The authors summation of the importance of this result is distinctly understated: "The ability to use scaling relationships to control product selectivity...has broad implications for molecular electrocatalysis". While the concept of thermodynamic bracketing is not novel to the study of chemical transformations, its implementation as a method for reaction control is underdeveloped for multielectron electrocatalytic conversions of small-molecule substrates.

4.4. Multimetallic Systems and Pendent Functionalities. Significant effort has been invested in the "rational" design of transition-metal complexes for interactions with oxygen, based on or inspired by features of metallocofactor structures in natural systems.[100] Initially, these structural modifications were intended to prevent the formation of bridging peroxo or oxo dimers following O_2 binding for systematic studies related to the function of oxygen carriers. As has been demonstrated in improving the activity of electrocatalysts for the hydrogen evolution reaction (HER)[101] and the CO_2 reduction reaction (CO2RR),[102] a sustained interest in the ability of $[Fe(TPP)]^+$ to function as a bioinspired mimic for the ORR capability of Cytochrome *c* oxidase continues to drive the design of ligand platforms with secondary sphere modifications to enhance reactivity and selectivity.[103,104] Similarly, multimetallic systems also continue to attract interest for the ORR,[105,106] because these also have parallels to the active sites of enzymes such as *laccase*.[107] Both of these design strategies have been shown to increase activity and selectivity for bioinspired systems. For instance, in unimolecular Co systems, where the selectivity for H_2O_2 is common,[108,109] dinuclear active sites and pendent functional groups have both proven to be successful strategies for driving product selectivity to H_2O instead.[52,110,111] However, as described in the Introduction, ORR by molecular electrocatalysts appears to exhibit a great sensitivity to other intrinsic factors like the electronic structure of the active species or the reaction medium.[30,49] Indeed, the secondary sphere effects can play a minor role relative to the driving force of the reaction, as determined by the formal reduction potential of the catalyst, depending on the overall reaction mechanism.[47]

The results presented above, summarizing the work of Stahl and co-workers,[99] are in contrast to the conclusions of an earlier study by Passard et al., who reported the observation of overpotential-dependent selectivity for two dicobalt catalyst systems.[53] In the case of these dicobalt systems, the authors explained that, although for all sacrificial proton donors used the reaction was at an overpotential for ORR to H_2O, it was only with strong acids that product selectivity became quantitative for H_2O. However, in considering the standard reduction potentials for ORR to H_2O and H_2O_2 (in both the MeCN and DMF solvents used), questions remain about this interpretation. As Stahl and co-workers harnessed in their experimental design, the formal potential for H_2O_2 is significantly negative of that for H_2O and the production of H_2O_2 can be thermodynamically excluded with sufficiently weak acids, provided the catalyst reduction potential is independent of proton activity. For instance, with the pK_a value for PhOH in MeCN of 27.2,[112] used by Passard et al.[53] in recalculating the standard potential for $O_2/H_2O_{2(MeCN)}$ using recently reported numbers[7,18] gives a value of −0.29 V vs NHE for H_2O_2, which is more negative than most of the electrochemical data where H_2O_2 production is reported (see the Methods section). For reasons of the complexity of anion solvation in MeCN, my lab and others[7,113] prefer the use of 29.14 for PhOH, obtained from the application of a self-consistent acidity scale.[114] This suggests that, at the reduction potential of both reported catalysts in MeCN (approximately equal to or more positive than 0.00 V vs NHE), experiments with added PhOH should be at counter-thermodynamic conditions for H_2O_2 production, when, in fact, these are the reaction conditions where the reported efficiency for this product is the greatest. The observation of catalytic activity for H_2O_2 in MeCN solution in this case might be attributed in part to the homoconjugation constant of PhOH increasing the effective acidity in solution. If the proton activity of unbuffered PhOH has a lower effective pK_a(MeCN) due to homoconjugation (alternatively reported as log K_f ($[(A)_2H]^-$) = 4.2 (ref 115) and 4.8 (ref 116)), the kinetic preference for H_2O_2 with weak acids would be thermodynamically viable.

Related questions arise for the reported DMF results:[53] the reported equilibrium constant for homoconjugation of log K_f ($[(A)_2H]^-$) = 3.8 (ref 116) for PhOH in DMF is within an order of magnitude of that reported in MeCN. Calculating the standard potential for $O_2/H_2O_{2(DMF)}$ provides a value of −0.36 V vs NHE with pK_a(PhOH) = 18.8 in DMF, which is more negative (counter-thermodynamic) of the reported catalytically active potentials in this solvent.[53] The selectivity difference between strong and weak acids in both solvent systems might reasonably be explained by a pK_a difference between the proximal and distal O atoms in the peroxo-containing intermediates for both catalysts. If an asymmetric peroxide binding mode occurs during the catalytic cycle, kinetic selectivity could be enabled when both products are

https://dx.doi.org/10.1021/acscatal.9b04477
ACS Catal. 2020, 10, 2640−2655

thermodynamically viable. Note that the stability of any H_2O_2 produced could be an issue with high concentrations of strong acid, especially if the catalysts are capable of catalase-type activity, which was not reported as a control in this study. Lastly, we note that, in our own studies, we were unable to obtain reliable RRDE data for H_2O_2 production with PhOH as a sacrificial proton donor, because of the competitive oxidation current generated by the conjugate phenolate base produced by proton consumption during a catalytic ORR response.[90,117]

Monte-Pérez et al. reported a multinuclear system that exhibited temperature-dependent product selectivity for H_2O/H_2O_2 at dinuclear Co sites within a larger multimetallic complex (Figure 9).[55] Temperature dependence on product selectivity

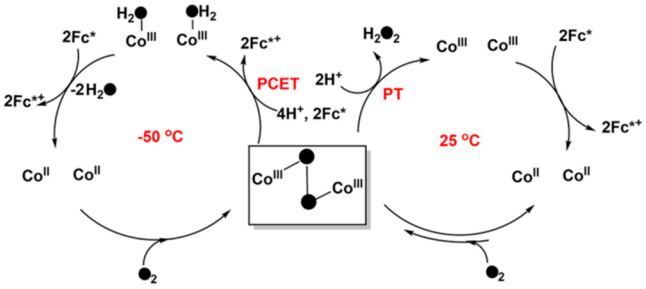

Figure 9. Proposed mechanisms of the temperature-dependent reduction of dioxygen to $4e^-/4H^+$ and $2e^-/2H^+$ products mediated by the dicobalt(II) units of a hexanuclear cobalt complex with a nonheme ligand system supported on a Sn_6O_6 stannoxane core. Fc* = decamethylferrocene, defined elsewhere as Cp^*_2Fe in this Perspective. [Reprinted with permission from ref 55. Copyright 2017, American Chemical Society, Washington, DC.]

was observed using Cp^*_2Fe as a solubilized chemical reductant and trifluoroacetic acid as a proton source. The complex contains six Co sites supported by a stannoxane core, which kinetic studies on the overall reaction suggest makes O_2 binding an entropically unfavorable process. The initial product of O_2 binding, a μ-1,2-peroxodicobalt(III) intermediate, is readily protonated at 25 °C, because of its instability. However, at −50 °C, where the intermediate has a greater thermodynamic stability, electron and proton donors have sufficient activity to complete conversion of the peroxo intermediate to 2 equiv of H_2O through successive proton-coupled electron transfer steps (Figure 9).

Following our observations on reductant-dependent mechanisms for ORR with a molecular Mn-based catalyst,[90,91] Wang et al. described a similar divergence between ORR pathways for a dinuclear Fe-based catalyst (see Figure 10).[54] In contrast to our own observations, however, the divergence was in selectivity for H_2O_2 vs H_2O when comparing chemical and electrochemical conditions. Despite significant efforts in this area, this study represents the first molecular nonheme iron-based ORR catalyst, suggesting there is much to gain through additional study on systems beyond the porphyrin ligand framework. Through mechanistic and computational studies, the authors found that the thiolate-rich ligand framework promotes the bimetallic activation of O_2 by two Fe centers. Interestingly, limited oxygenation of the thiolate moieties of the catalyst construct occurs during catalysis, suggesting they are difficult to oxidize under these conditions, which is rationalized by the relative absence of spin density on S in electronic structure calculations. Similar to our own studies, where O atom protonation can act as a relay to reduced O_2 species, thiolate

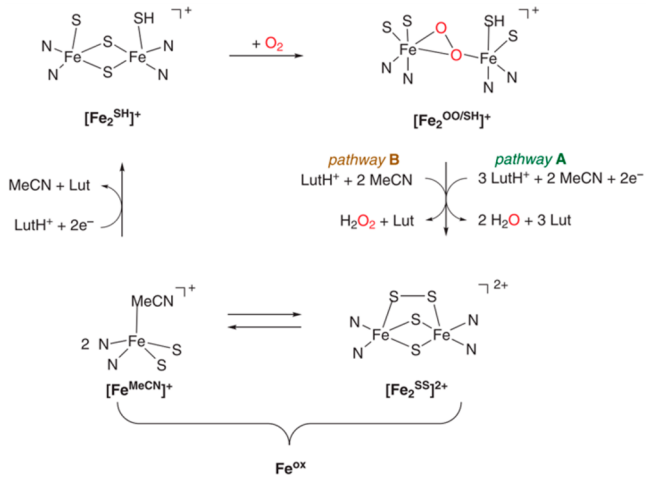

Figure 10. Proposed $4H^+/4e^-$ (electrochemically driven) and $2H^+/2e^-$ (chemical reducing agent) catalytic O_2 reduction pathways. $LutH^+$ = 2,6-lutidinium tetrafluoroborate acid. [Adapted with permission from ref 54. Copyright 2019, American Chemical Society, Washington, DC.]

protonation is proposed to be an integral mechanistic component. As Wang et al. have noted, there are relatively few examples of analogous behavior with O and N atom donors and even fewer with S, rendering generalization to specific trends difficult. However, it is clear that proton sensitivity of heteroatoms in the ligand coordination sphere can play an important role in catalytic activity. The divergent product selectivity is rationalized as a function of how "reducing" the chemical environment is, since increasing the concentration of dissolved chemical reductant decreases the amount of H_2O_2 generated during the catalytic reaction. Similar to our own studies on mechanistic divergence, Wang et al. suggested that the reaction-diffusion layer under electrocatalytic conditions can drive catalytic multielectron processes more efficiently when sequential reduction steps require additional reducing power. In this report, only conditions where both H_2O- and H_2O_2-producing reactions are thermodynamically viable were used.

Substantial work has been done on bimetallic and pendent functional-group-containing catalyst constructs in the context of ORR. Fe and Co complexes with pendent functional groups, as well as related bimetallic constructs, have all been shown to impact selectivity and activity for the ORR, both through strictly inductive effects and by modifying the preferred reaction pathway.[46−56,103,118,119] These strategies can mitigate the intrinsic preferences of mononuclear catalysts: single-site Co centers generally prefer the production of H_2O_2,[108,109] but the inclusion of a second catalyst center can provide the remaining two electron equivalents required to generate H_2O.[8,56,119,120] Fukuzumi and co-workers have reported a Cu-based catalyst with a modified *tris*(2-pyridylmethyl)amine ligand that is selective for H_2O with weak acids.[121] The inclusion of a bulky pivalamido group on one of the pyridine moieties partially blocks the first coordination sphere of the Cu center, allowing O_2 and HO_2^- binding, but restricting the access of the bulkier trifluoroacetate anion generated by proton consumption during catalysis.

Dey and co-workers have published a series of studies on abiotic constructs intended to mimic the function and properties of Fe-containing heme metallocofactors for ORR.[50,89,103] One study of relevance to the discussion of bimetallic active sites examined the electrocatalytic properties of a synthetic heme

https://dx.doi.org/10.1021/acscatal.9b04477
ACS Catal. 2020, 10, 2640−2655

Cytochrome *c* oxidase mimic.[122] A series of derivatives were prepared that systematically examined the role of Cu in the binuclear active site, as well as the role of imidazole coordination in a position *trans* to the bimetallic O_2 binding pocket as an analogue of histidine in the conserved active site. By immobilizing the bimetallic catalyst construct on a roughened Ag surface using self-assembled monolayers, they were able to obtain spectroelectrochemical surface-enhanced resonance Raman data, in static and rotating electrode configurations. Interestingly, the imidazole-containing bimetallic compound was less active and selective for the $4e^-/4H^+$ reduction product H_2O than the imidazole-free bimetallic Cu−Fe species. The authors ascribe the differences in activity and efficiency to slow ligand exchange from an intermediate low-spin Fe(II) species; imidazole is enough of a strong-field ligand under these reducing conditions to alter electrochemical speciation by inhibiting rapid ligand exchange at the bimetallic active site.

A continuing challenge for molecular inorganic complexes in ORR is solubilizing them for study under aqueous conditions.[87,123] A recent report from Liu et al. described the catalytic properties of a dinuclear copper catalyst that demonstrated activity for H_2O in both DMF with an added proton donor and in buffered aqueous solutions.[124] Mechanistic studies suggested that stepwise reduction of the Cu sites occurred on the reported CV time scales, resulting in the formation of an intermediate mixed-valent Cu^{II}/Cu^{I} species that could activate dissolved O_2 to superoxide to initiate the catalytic cycle. The authors reported peak efficiency for water at pH 7 across a range of pH 5−9 and suggested that further study was required to elucidate whether homolytic or heterolytic cleavage of the O−O bond was occurring during the catalytic cycle. The pK_a values of probable aquo species were not quantified to compare with the pH-dependent catalytic efficiency results, but the absence of a reversible electrochemical response under aqueous conditions precludes a rigorous Pourbaix-type analysis. In our own studies under aqueous conditions with a homogeneous single-site Mn(porphyrin)-based electrocatalyst, the reversibility of the electrochemical response, coupled with redox-diagnostic absorbance properties, allowed a thorough mechanistic cycle to be built using electroanalytical and ultraviolet−visible light (UV-vis) spectroelectrochemical techniques.[87] UV-vis spectroelectrochemistry is uniquely positioned to study homogeneous catalyst systems with charge-transfer bands in the visible region in aqueous solvent systems.[125]

Clearly, multimetallic active sites can alter selectivity from their monometallic analogues, generally by enabling alternate bimetallic reduction pathways, a strategy inspired by well-studied bioinorganic cofactors capable of a much larger scope of redox-based small molecule transformations. The challenge to developing new multimetallic molecular catalysts for O_2 reduction is the significant possible parameter space. Unlike pendent functional groups, where the effects of relatively simple modifications like the inclusion of an acidic proton donor or relay moiety can be tested,[109] there are many possible combinations for heterobimetallic systems to assess in any given dinuclear catalyst framework. A related challenge to the potential scope of bimetallic constructs is the difficulty of synthesizing heterobimetallic catalyst species, especially when coordination sites and metal ions are capable of engaging in multiple—and, therefore, nonspecific—interactions with each other. An ongoing challenge for this area is the development of more straightforward routes to heterobimetallic species to improve our fundamental understanding of how heterobimetallic catalysts can be developed and optimized. As discussed above, the asymmetry of O_2 activation has clear consequences on product selectivity, which implies a significant possible benefit for well-designed heterobimetallic active sites in the ORR.

4.5. Electron−Proton Transfer Mediators and Product Selectivity. In biological systems, quinone moieties participate in electron and proton transfer pathways. One example is ubiquinone, which participates in the redox cascade of Cytochrome *c* oxidase (see Scheme 3A).[126] Because of their ability to function as efficient $2e^-/2H^+$ transfer agents, they have also found utility in the catalytic aerobic oxidation of small organic molecules (Scheme 3B).[127−129] Inspired by these precedents, Anson and Stahl undertook a series of studies on using quinone as an electron−proton transfer mediator (EPTM) as part of a cooperative catalytic system with a molecular Co complex, Co(salophen) (Scheme 3C).[57] Under suitable reaction conditions, excess *p*-hydroquinone can serve as a source of electrons and protons to reduce O_2 when a cobalt(II) salophen compound is present.[58] However, the key discovery was that it was possible to take advantage of the intrinsic $2e^-/2H^+$ electrochemical activity of the *p*-benzoquinone/*p*-hydroquinone couple to develop a truly co-catalytic system. Under co-catalytic conditions, with *p*-benzoquinone/*p*-hydroquinone functioning as an EPTM, binding and activation of O_2 by Co(salophen) resulted in a Co-superoxide species, which could undergo consecutive reductions by electrogenerated *p*-hydroquinone to H_2O_2 and then H_2O. Electrochemical co-catalytic reaction conditions included an excess of a sacrificial proton donor and the redox potential of the Co(salophen) is well-matched with that of *p*-benzoquinone/*p*-hydroquinone, such that regeneration of the active species occurred rapidly with respect to the rate of the co-catalytic reaction. It was possible to observe distinct changes in the kinetic response of the combined system by CV (Scheme 3C). Separate thermal catalytic (Co(salophen) with O_2 and *p*-hydroquinone) experiments

Scheme 3. O_2 Reduction Mediated by Quinones (Red) and Macrocyclic Metal Complexes (Blue)[a]

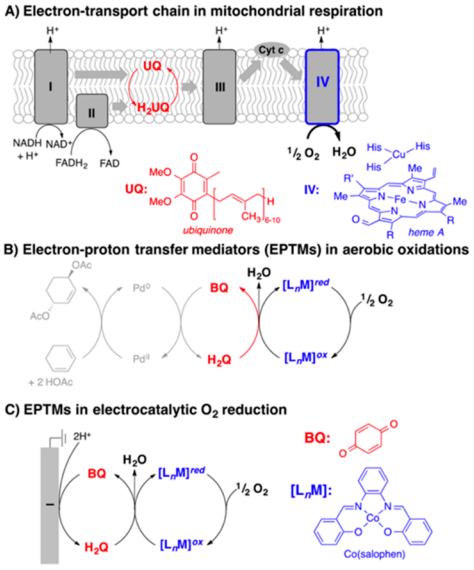

[a][Reproduced with permission from ref 57. Copyright 2017, American Chemical Society, Washington, DC.]

https://dx.doi.org/10.1021/acscatal.9b04477
ACS Catal. 2020, 10, 2640−2655

analyzed by O_2 uptake experiments and controlled potential electrolysis experiments run under constant O_2 purging were conducted to support the existence of the proposed co-catalytic behavior.[57]

In addition to their co-catalytic function, the inclusion of quinones also alters the selectivity of the reaction. As discussed above, many Co-based systems demonstrate high electrocatalytic selectivity for H_2O_2.[108] Under general electrocatalytic conditions, Co(salophen) also produces H_2O_2 selectively, it is only with the *p*-benzoquinone/*p*-hydroquinone EPTM present that selectivity shifts exclusively to H_2O. Stahl and co-workers were able to show several viable molecular inorganic catalyst-EPTM pairs that functioned along this general scheme,[57] but questions remain about the role of redox pairing and how the nature of interactions between the reduced *p*-hydroquinone and the catalyst *prior* to O_2 binding can be used as a point of reaction control. It is clear, however, that redox mediators, which often function at potentials and acidities relevant to small-molecule activation, represent a paradigmatic shift in the design of electrocatalytic processes and hold new opportunities for future development. However, the study of related co-catalyst systems requires caution, since a rigorous understanding of mediator and catalyst function is required *before* examining the combined system, with the additional caveat that distinguishing between overlapping and distinct catalytic processes may be nontrivial. If the redox-driven mediator activation response is not fast relative to substrate activation by the catalyst, any description of emergent effects may be incorrect. Lastly, although intrinsic mediator redox activity can be the result of CPET processes, it should be acknowledged that this does not require that every elementary step in the (co)catalytic cycle should have the same kinetic preference for the EPTM to enhance the reaction.

5. DISCUSSION AND FUTURE CHALLENGES

The recent results highlighted here are a promising indication of new directions in the field. The advent of new H_2O_2-selective catalysts suggests that continued study in this area is enabling the development of a nuanced understanding of reaction control. This is also reflected in the ubiquity of mechanistic experiments where the choice of reductant or temperature shifts selectivity and mechanism. New experimental designs have resulted in paradigmatic shifts by introducing both thermodynamic bracketing and EPTMs as a point-of-control for reaction selectivity and activity.

Although many of the studies highlighted here demonstrate excellent work on understanding and controlling the thermodynamic aspects of the electrocatalytic reduction of O_2 at molecular active sites, there are continued challenges for the field. In comparison to active heterogeneous materials, molecular systems often do not demonstrate competent activity at low driving forces (overpotentials). Considering the activity of homogeneous and heterogeneous catalysts in the same reaction medium, diffusional limitations inherent to a molecular catalytic process are also limiting, in comparison to insoluble materials, because of the generation of O_2 concentration gradients near the electrode surface where the precatalyst in solution must be activated. The inclusion of strong Lewis bases such as imidazole are known to improve the favorability of O_2 binding, but corresponding increases in stability for other intermediates can slow the overall rate of reaction considerably, which was observed in the study of the Cytochrome *c* oxidase mimic discussed above.[122] This is an effect akin to the scaling relationships and "volcano" plots often discussed for heterogeneous systems: perturbing the stability or activity at one point in the system can and will necessarily modify the energy of intermediates at different points on the reaction coordinate as well. Dey and co-workers noted that, by greatly improving O_2 binding, the system had diminished ability to rapidly release water, because of the improved stability of the low-spin Fe(II) octahedral coordination environment.[122]

The use of apparent scaling relationships in molecular electrocatalyst systems can be used to alter catalytic performance,[47,49,99,130] although Costentin and Savéant have argued that a "first-principles" connection between the reaction "driving force" and the fundamental kinetic response cannot be deduced *a priori* for the electrocatalytic response, when considering the "standard" state of the reaction.[131] *This does not mean that, at nonstandard states (often the experimentally achievable reaction conditions), the explicit tuning and optimization of the catalytic response is not possible or an essential mode of control.* In contrast, the underlying Nernstian reactions that control the potential of catalyst activation through equilibrium substrate binding steps are intrinsically sensitive to concentration variance.[47] Furthermore, changes in catalyst speciation (either through explicit tuning of the reaction driving force through proton activity or the alteration of catalyst and substrate concentrations) will change the basic nature of the potential energy surface of the catalytic reaction. This is directly evident in the recent report by Pegis et al., where it was shown that the $[Fe(TPP)]^+$ precatalyst could vary between *three different resting states* over the course of the reaction, as shifting equilibria and speciation altered the kinetic catalytic response.[45]

Similar effects of concentration can alter the kinetic response achieved according to the catalytic rate law, since apparent reaction rates are, by nature, responsive to substrate availability. As mentioned above, from a "standard states" perspective, Costentin and Savéant have argued that the connection between the fundamental kinetic rate of any multistep catalytic reaction at standard states can only be directly linked through a first-principles kinetic and thermodynamic reaction analysis to the highest free-energy barrier.[131] However, a survey of the results discussed here shows that it is not common to find catalyst systems that are stable and functional at the "standard" acid concentration of 1 M. Since these conditions often cannot be directly measured, it is unclear whether the kinetic rate-defining $E_{1/2}$ value of the catalyst would remain unaltered. It is also possible for any given catalyst that the most active species may simply not exist at the standard state.

In all of the cases described above, careful mechanistic study showed that nuanced interactions between reaction components and byproducts impart complexity to reaction profiles; some of these interactions are capable of dynamically shifting the overall system between different catalytic pathways as the reaction proceeds. ORR by the systems described in these reports also doesn't require formally zero-valent metal centers, instead displaying catalytic responses from divalent metal centers that are inherently susceptible to binding interactions with the conjugate bases of any sacrificial proton donors that will alter catalyst speciation over time. Essential to this complexity is an opportunity for the field to use "real-world" (specifically "nonstandard") conditions to identify extraordinary activity through precise control of reaction speciation and reagent/reactant concentrations.

This is illustrated in the case of the $[Co(por^{OMe})]$ catalyst discussed above (recall Figure 8), where the correlation between pK_a and reaction barriers for H_2O_2 and O_2 is evident with strong

https://dx.doi.org/10.1021/acscatal.9b04477
ACS Catal. 2020, 10, 2640−2655

acids present.[99] Although both reactions are thermodynamically allowed under these conditions, the production of H_2O_2 is favored via a lower kinetic barrier, although it occurs with a lower "driving force".[99] In the presence of weak acids, the production of H_2O_2 is thermodynamically bracketed from occurring, shifting product selectivity exclusively to H_2O. The concomitant change in the experimentally observed rate law is consistent with a change in the elementary step of the reaction between the two reaction conditions, as is the change in slope observed for the pK_a(DMF) vs log(TOF, s^{-1}) plot.[99]

The report on EPTMs from Anson and Stahl is particularly intriguing for controlling reaction conditions.[57] It is not clear yet from these data, however, what design rules exist for choosing EPTMs for specific ORR catalysts. Since the original report demonstrated that *p*-hydroquinone could reduce the readily formed Co(III)(salophen) superoxide species,[58] a key component of co-catalytic activity for the ORR could be the ability of the EPTM to act upon intermediate metal superoxides. As mentioned above, under the reaction conditions studied, the CPET activation of the mediator is anticipated to have rates which are greatly in excess of any CPET reactions related to the catalytic response, but it is not obvious what the relationship of this difference to the efficiency and activity of a given catalytic system is, or if acting on CPET steps intrinsic to the catalyst function is a core component of the emergent activity of the combined catalyst/mediator system at all. Answering these questions could have general applicability to the design of EPTMs as (co)catalysts for a variety of small-molecule reactions.

Our own observations of pre-equilibrium catalyst tuning raises questions about how modifying the thermochemical relationship between activated intermediates on either side of the rate-determining step could be used to enhance catalytic rates. Pegis et al. were forced to exclude the *meso*-2-pyridyl derivative of the $[Fe(porphyrin)]^+$ system from some of their analyses, because the Nernstian shift of the Fe(III)/(II) reduction potential with increasing acid concentration caused a corresponding decrease in the catalytic rate.[47] That is, increasing acid concentrations were changing the speciation of the Fe precatalyst prior to reduction, with corresponding effects on the $E_{1/2}$ value that is directly linked to the reaction rate. This suggests the possibility that pre-equilibrium effects which push the $E_{1/2}$ to more negative potentials could result in concentration-dependent rate increases. We are currently investigating a related question about the nature of our own Mn-based catalyst, where increasing concentrations of weak acids cause a general increase in the observed catalytic current response, even as the $E_{1/2}$ shifts to more positive potentials in a Nernstian manner.[90] This apparent decoupling of the expected relationship between activity to the catalyst $E_{1/2}$ is suggestive of additional speciation effects altering the relative energetic positioning and equilibria of intermediate species in the catalytic cycle, with related changes in the observed kinetic response. A better understanding of this phenomenon generally could lead to groundbreaking catalyst *systems* through reaction control, where the addition of substrate tunes the catalyst to low overpotentials while dramatically increasing the observed activity. This possibility is made all the more intriguing by the observation that the use of buffered acids to thermodynamically constrain our Mn-based catalyst *shows the expected relationship of catalyst $E_{1/2}$ and reaction standard potential to observed activity*, indicating that, at sufficient concentrations, anionic phenolate derivatives have an important role on catalyst speciation as it relates to the catalytic response.[91]

Finally, the construction of new homobimetallic and heterobimetallic molecular catalysts would benefit from the incorporation of assembly methods beyond static covalent bonds. Competent bimetallic catalysts which use dynamic covalent bonds, supramolecular effects, and hydrogen-bonding interactions have been successfully implemented in the study of other redox-based catalytic processes involving small molecules.[132−136] Bimetallic bridging peroxide formation is well-known for nominally unimolecular transition-metal complexes capable of O_2 binding and activation, which represents an opportunity to study the effects of "soft" interactions on the assembly and reactivity of intermediates. For instance, controlling the reaction pathway to dimer formation and using noncovalent interactions between the ligand framework and the bound peroxide to weaken the O−O bond in an intermediate peroxide would be expected have profound effects on the catalytic competency of these systems.[137,138] The importance of similar modifications has been elucidated experimentally in the more statically assembled systems discussed here, which is suggestive of the viability of this hypothesis.[54,55]

6. CONCLUSIONS AND OUTLOOK

These recent studies suggest that there is a continuing benefit to the study of the molecular electrocatalytic reduction of O_2. The mechanistic fundamentals of homogeneous O_2 activation have relevance to the understanding of biological systems, as well as the development of better ORR and aerobic oxidation catalysts.[7,139−143] There is sustained interest in running the latter electrochemically,[144−146] given the obvious parallels to the function of *Cytochrome* P450,[21−23] which catalyzes the oxygenation of endogenous and exogenous molecules to produce important metabolites. Mechanistic and thermodynamic understanding of molecular catalysis can be the basis of intriguing systems with careful experimental design: a recent study combined Rh porphyrins with methane and O_2 to assemble an abiotic system capable of activity analogous to methane monooxygenase by exploiting electrochemically generated reaction gradients created by inorganic nanomaterials.[147] Innovation in the area of multicomponent systems leveraging molecular control will continue to advance areas related to reductive O_2 activation as mechanistic understanding provides new insight.

7. METHODS

7.1. Computational Methods. DFT calculations were performed on the Rivanna High-Performance Computing Cluster at the University of Virginia, using ORCA 4.2.1.[73] Geometry optimizations were performed unrestricted with the B3LYP/G[74−78] functional and def2-SVP[79,80] basis set with the RIJCOSX approximation,[81] D3BJ dispersion correction,[82,83] and CPCM[84] to model solvation by MeCN and DMF. Numerical frequency calculations were performed with a def2-SVP[79,80] basis set to validate the optimized geometries as minima on the potential energy surface and to generate thermochemical data. All images were generated using Chimera.[148]

7.2. Standard Potential Calculations. Standard potential values for ORR to H_2O and H_2O_2 in MeCN and DMF were calculated using eqs 1−4 (referenced to Fc^+/Fc[7]) for comparison with the results of Passard et al.[53] We note that a general agreement is achieved for the standard potentials of O_2 to H_2O, but the H_2O_2 values suggest counterthermodynamic

https://dx.doi.org/10.1021/acscatal.9b04477
ACS Catal. 2020, 10, 2640−2655

conditions, unless homoconjugation of PhOH increases its effective acidity.

$$O_{2(g)} + 2HA_{(MeCN)} + 2e^- \rightleftharpoons H_2O_{2(MeCN)} + 2A^-$$
$$E^0 = [0.68 - 0.0592pK_{a(MeCN)}(HA)] \quad (1)$$

$$O_{2(g)} + 2HA_{(DMF)} + 2e^- \rightleftharpoons H_2O_{2(DMF)} + 2A^-$$
$$E^0 = [0.06 - 0.0592pK_{a(DMF)}(HA)] \quad (2)$$

$$O_{2(g)} + 4HA_{(MeCN)} + 4e^- \rightleftharpoons 2H_2O_{(MeCN)} + 4A^-$$
$$E^0 = [1.21 - 0.0592pK_{a(MeCN)}(HA)] \quad (3)$$

$$O_{2(g)} + 4HA_{(DMF)} + 4e^- \rightleftharpoons 2H_2O_{(DMF)} + 4A^-$$
$$E^0 = [0.60 - 0.0592pK_{a(DMF)}(HA)] \quad (4)$$

The standard Fc^+/Fc potential in MeCN was referenced as +0.64 V, with respect to NHE.[149,150] In DMF, the standard Fc^+/Fc potential was referenced as +0.69 V, with respect to NHE;[149] SCE was referenced as +0.24 V, with respect to NHE.[151]

product	solvent	standard potential w/PhOH vs NHE[a]	standard potential w/PhOH vs NHE[b]
H_2O_2	MeCN	−0.29	n/a
H_2O	MeCN	+0.24	+0.430
H_2O_2	DMF	−0.36	n/a
H_2O	DMF	+0.18	−0.301

In the above-noted array, footnote *a* indicates that pK_a(PhOH) 27.2 in MeCN,[112] using the standard potentials of Mayer and coworkers.[7,18] Notably, for reasons of the complexity of anion solvation in MeCN, we and others[7,113] prefer the use of 29.14 for PhOH, obtained from the application of a self-consistent acidity scale.[114] pK_a(PhOH) 18.8 in DMF.[7,53] Footnote *b* indicates that values were provided by Passard et al.[53]

■ ASSOCIATED CONTENT

Supporting Information

The Supporting Information is available free of charge at https://pubs.acs.org/doi/10.1021/acscatal.9b04477.

Coordinates, selected QRO energies, Mulliken charges, and Loewdin charges of $[Fe(TPP)(\eta^1\text{-}O_2^{\bullet-})(1\text{-MeIm})]^0$ and $[Co(TPP)(\eta^1\text{-}O_2^{\bullet-})(1\text{-MeIm})]^0$ (PDF)

■ AUTHOR INFORMATION

Corresponding Author

Charles W. Machan − *University of Virginia, Charlottesville, Virginia 22904-4319, United States;* orcid.org/0000-0002-5182-1138; Email: machan@virginia.edu

Complete contact information is available at: https://pubs.acs.org/10.1021/acscatal.9b04477

Notes

The author declares no competing financial interest.

■ ACKNOWLEDGMENTS

I thank Dr. Cyrille Costentin and an anonymous reviewer for helpful discussion and criticism concerning the summaries and viewpoints contained in this Perspective.

■ REFERENCES

(1) Sahu, S.; Goldberg, D. P. Activation of Dioxygen by Iron and Manganese Complexes: A Heme and Nonheme Perspective. *J. Am. Chem. Soc.* **2016**, *138*, 11410−28.

(2) Sono, M.; Roach, M. P.; Coulter, E. D.; Dawson, J. H. Heme-Containing Oxygenases. *Chem. Rev.* **1996**, *96*, 2841−2888.

(3) Wallar, B. J.; Lipscomb, J. D. Dioxygen Activation by Enzymes Containing Binuclear Non-Heme Iron Clusters. *Chem. Rev.* **1996**, *96*, 2625−2658.

(4) Dey, S.; Mondal, B.; Chatterjee, S.; Rana, A.; Amanullah, S.; Dey, A. Molecular electrocatalysts for the oxygen reduction reaction. *Nat. Rev. Chem.* **2017**, *1*, 0098.

(5) Kulkarni, A.; Siahrostami, S.; Patel, A.; Nørskov, J. K. Understanding Catalytic Activity Trends in the Oxygen Reduction Reaction. *Chem. Rev.* **2018**, *118*, 2302−2312.

(6) Jasniewski, A. J.; Que, L. Dioxygen Activation by Nonheme Diiron Enzymes: Diverse Dioxygen Adducts, High-Valent Intermediates, and Related Model Complexes. *Chem. Rev.* **2018**, *118*, 2554.

(7) Pegis, M. L.; Wise, C. F.; Martin, D. J.; Mayer, J. M. Oxygen Reduction by Homogeneous Molecular Catalysts and Electrocatalysts. *Chem. Rev.* **2018**, *118*, 2340−2391.

(8) Zhang, W.; Lai, W.; Cao, R. Energy-Related Small Molecule Activation Reactions: Oxygen Reduction and Hydrogen and Oxygen Evolution Reactions Catalyzed by Porphyrin- and Corrole-Based Systems. *Chem. Rev.* **2017**, *117*, 3717−3797.

(9) Rice, D. B.; Massie, A. A.; Jackson, T. A. Manganese−Oxygen Intermediates in O−O Bond Activation and Hydrogen-Atom Transfer Reactions. *Acc. Chem. Res.* **2017**, *50*, 2706−2717.

(10) Khan, A.; Gunawan, C. A.; Zhao, C. Oxygen Reduction Reaction in Ionic Liquids: Fundamentals and Applications in Energy and Sensors. *ACS Sustainable Chem. Eng.* **2017**, *5*, 3698−3715.

(11) Elwell, C. E.; Gagnon, N. L.; Neisen, B. D.; Dhar, D.; Spaeth, A. D.; Yee, G. M.; Tolman, W. B. Copper−Oxygen Complexes Revisited: Structures, Spectroscopy, and Reactivity. *Chem. Rev.* **2017**, *117*, 2059−2107.

(12) Baglia, R. A.; Zaragoza, J. P. T.; Goldberg, D. P. Biomimetic Reactivity of Oxygen-Derived Manganese and Iron Porphyrinoid Complexes. *Chem. Rev.* **2017**, *117*, 13320−13352.

(13) Shao, M.; Chang, Q.; Dodelet, J.-P.; Chenitz, R. Recent Advances in Electrocatalysts for Oxygen Reduction Reaction. *Chem. Rev.* **2016**, *116*, 3594−3657.

(14) Viswanathan, V.; Hansen, H. A.; Rossmeisl, J.; Nørskov, J. K. Universality in Oxygen Reduction Electrocatalysis on Metal Surfaces. *ACS Catal.* **2012**, *2*, 1654−1660.

(15) Saouma, C. T.; Mayer, J. M. Do spin state and spin density affect hydrogen atom transfer reactivity? *Chemical Science* **2014**, *5*, 21−31.

(16) Goetz, M. K.; Anderson, J. S. Experimental Evidence for pKa-Driven Asynchronicity in C−H Activation by a Terminal Co(III)−Oxo Complex. *J. Am. Chem. Soc.* **2019**, *141*, 4051−4062.

(17) Huang, T.; Rountree, E. S.; Traywick, A. P.; Bayoumi, M.; Dempsey, J. L. Switching between Stepwise and Concerted Proton-Coupled Electron Transfer Pathways in Tungsten Hydride Activation. *J. Am. Chem. Soc.* **2018**, *140*, 14655−14669.

(18) Pegis, M. L.; Roberts, J. A. S.; Wasylenko, D. J.; Mader, E. A.; Appel, A. M.; Mayer, J. M. Standard Reduction Potentials for Oxygen and Carbon Dioxide Couples in Acetonitrile and N,N-Dimethylformamide. *Inorg. Chem.* **2015**, *54*, 11883−11888.

(19) Wood, P. M. The potential diagram for oxygen at pH 7. *Biochem. J.* **1988**, *253*, 287−289.

(20) Collman, J. P.; Boulatov, R.; Sunderland, C. J.; Fu, L. Functional analogues of cytochrome c oxidase, myoglobin, and hemoglobin. *Chem. Rev.* **2004**, *104*, 561−588.

(21) Denisov, I. G.; Makris, T. M.; Sligar, S. G.; Schlichting, I. Structure and Chemistry of Cytochrome P450. *Chem. Rev.* **2005**, *105*, 2253−2278.

(22) Feiters, M. C.; Rowan, A. E.; Nolte, R. J. M. From simple to supramolecular cytochrome P450 mimics. *Chem. Soc. Rev.* **2000**, *29*, 375−384.

(23) Schlichting, I.; Berendzen, J.; Chu, K.; Stock, A. M.; Maves, S. A.; Benson, D. E.; Sweet, R. M.; Ringe, D.; Petsko, G. A.; Sligar, S. G. The Catalytic Pathway of Cytochrome P450cam at Atomic Resolution. *Science* **2000**, *287*, 1615−1622.
(24) Zagal, J. H.; Koper, M. T. M. Reactivity Descriptors for the Activity of Molecular MN4 Catalysts for the Oxygen Reduction Reaction. *Angew. Chem., Int. Ed.* **2016**, *55*, 14510−14521.
(25) Costas, M.; Mehn, M. P.; Jensen, M. P.; Que, L. Dioxygen Activation at Mononuclear Nonheme Iron Active Sites: Enzymes, Models, and Intermediates. *Chem. Rev.* **2004**, *104*, 939−986.
(26) Que, L.; Ho, R. Y. N. Dioxygen Activation by Enzymes with Mononuclear Non-Heme Iron Active Sites. *Chem. Rev.* **1996**, *96*, 2607−2624.
(27) Vogt, L. H.; Faigenbaum, H. M.; Wiberly, S. E. Synthetic Reversible Oxygen-Carrying Chelates. *Chem. Rev.* **1963**, *63*, 269−277.
(28) Jones, R. D.; Summerville, D. A.; Basolo, F. Synthetic oxygen carriers related to biological systems. *Chem. Rev.* **1979**, *79*, 139−179.
(29) Momenteau, M.; Reed, C. A. Synthetic Heme-Dioxygen Complexes. *Chem. Rev.* **1994**, *94*, 659−698.
(30) Costentin, C.; Savéant, J.-M. Towards an intelligent design of molecular electrocatalysts. *Nat. Rev. Chem.* **2017**, *1*, 0087.
(31) Basolo, F.; Hoffman, B. M.; Ibers, J. A. Synthetic oxygen carriers of biological interest. *Acc. Chem. Res.* **1975**, *8*, 384−392.
(32) Vaska, L. Dioxygen-metal complexes: toward a unified view. *Acc. Chem. Res.* **1976**, *9*, 175−183.
(33) Lei, H.; Li, X.; Meng, J.; Zheng, H.; Zhang, W.; Cao, R. Structure Effects of Metal Corroles on Energy-Related Small Molecule Activation Reactions. *ACS Catal.* **2019**, *9*, 4320−4344.
(34) Lei, H.; Liu, C.; Wang, Z.; Zhang, Z.; Zhang, M.; Chang, X.; Zhang, W.; Cao, R. Noncovalent Immobilization of a Pyrene-Modified Cobalt Corrole on Carbon Supports for Enhanced Electrocatalytic Oxygen Reduction and Oxygen Evolution in Aqueous Solutions. *ACS Catal.* **2016**, *6*, 6429−6437.
(35) Meng, J.; Lei, H.; Li, X.; Qi, J.; Zhang, W.; Cao, R. Attaching Cobalt Corroles onto Carbon Nanotubes: Verification of Four-Electron Oxygen Reduction by Mononuclear Cobalt Complexes with Significantly Improved Efficiency. *ACS Catal.* **2019**, *9*, 4551−4560.
(36) Xie, L.; Li, X.; Wang, B.; Meng, J.; Lei, H.; Zhang, W.; Cao, R. Molecular Engineering of a 3D Self-Supported Electrode for Oxygen Electrocatalysis in Neutral Media. *Angew. Chem., Int. Ed.* **2019**, *58*, 18883−18887.
(37) Fremy, E. Untersuchungen über das Kobalt. *Jus. Lieb. Ann. Chem.* **1852**, *83*, 227−249.
(38) Pfeiffer, P.; Breith, E.; Lübbe, E.; Tsumaki, T. Tricyclische orthokondensierte Nebenvalenzringe. *Jus. Lieb. Ann. Chem.* **1933**, *503*, 84−130.
(39) Tsumaki, T. Nebenvalenzringverbindungen. IV. Über einige innerkomplexe Kobaltsalze der Oxyaldimine. *Bull. Chem. Soc. Jpn.* **1938**, *13*, 252−260.
(40) Pauling, L.; Coryell, C. D. The Magnetic Properties and Structure of Hemoglobin, Oxyhemoglobin and Carbonmonoxyhemoglobin. *Proc. Natl. Acad. Sci. U. S. A.* **1936**, *22*, 210.
(41) Fogler, B. B. PILOT PLANTS: Regenerative Unit for Generating Oxygen. *Ind. Eng. Chem.* **1947**, *39*, 1353−1360.
(42) Vannerberg, N. G.; Brosset, C. The crystal structure of decammine-μ-peroxodicobalt pentanitrate. *Acta Crystallogr.* **1963**, *16*, 247−251.
(43) Vaska, L. Oxygen-Carrying Properties of a Simple Synthetic System. *Science* **1963**, *140*, 809.
(44) Ibers, J. A.; La Placa, S. J. Molecular Structure of the Synthetic Molecular Oxygen Carrier $O_2IrCl(CO)(P[C_6H_5]_3)_2$. *Science* **1964**, *145*, 920.
(45) Pegis, M. L.; Martin, D. J.; Wise, C. F.; Brezny, A. C.; Johnson, S. I.; Johnson, L. E.; Kumar, N.; Raugei, S.; Mayer, J. M. Mechanism of Catalytic O_2 Reduction by Iron Tetraphenylporphyrin. *J. Am. Chem. Soc.* **2019**, *141*, 8315−8326.
(46) Carver, C. T.; Matson, B. D.; Mayer, J. M. Electrocatalytic Oxygen Reduction by Iron Tetra-arylporphyrins Bearing Pendant Proton Relays. *J. Am. Chem. Soc.* **2012**, *134*, 5444−5447.
(47) Pegis, M. L.; McKeown, B. A.; Kumar, N.; Lang, K.; Wasylenko, D. J.; Zhang, X. P.; Raugei, S.; Mayer, J. M. Homogenous Electrocatalytic Oxygen Reduction Rates Correlate with Reaction Overpotential in Acidic Organic Solutions. *ACS Cent. Sci.* **2016**, *2*, 850−856.
(48) Matson, B. D.; Carver, C. T.; Von Ruden, A.; Yang, J. Y.; Raugei, S.; Mayer, J. M. Distant protonated pyridine groups in water-soluble iron porphyrin electrocatalysts promote selective oxygen reduction to water. *Chem. Commun.* **2012**, *48*, 11100−11102.
(49) Rigsby, M. L.; Wasylenko, D. J.; Pegis, M. L.; Mayer, J. M. Medium Effects Are as Important as Catalyst Design for Selectivity in Electrocatalytic Oxygen Reduction by Iron−Porphyrin Complexes. *J. Am. Chem. Soc.* **2015**, *137*, 4296−4299.
(50) Mukherjee, S.; Mukherjee, M.; Mukherjee, A.; Bhagi-Damodaran, A.; Lu, Y.; Dey, A. O_2 Reduction by Biosynthetic Models of Cytochrome c Oxidase: Insights into Role of Proton Transfer Residues from Perturbed Active Sites Models of CcO. *ACS Catal.* **2018**, *8*, 8915−8924.
(51) Passard, G.; Dogutan, D. K.; Qiu, M.; Costentin, C.; Nocera, D. G. Oxygen reduction reaction promoted by manganese porphyrins. *ACS Catal.* **2018**, *8*, 8671−8679.
(52) McGuire, R., Jr; Dogutan, D. K.; Teets, T. S.; Suntivich, J.; Shao-Horn, Y.; Nocera, D. G. Oxygen reduction reactivity of cobalt(ii) hangman porphyrins. *Chem. Sci.* **2010**, *1*, 411−414.
(53) Passard, G.; Ullman, A. M.; Brodsky, C. N.; Nocera, D. G. Oxygen Reduction Catalysis at a Dicobalt Center: The Relationship of Faradaic Efficiency to Overpotential. *J. Am. Chem. Soc.* **2016**, *138*, 2925−2928.
(54) Wang, L.; Gennari, M.; Cantú Reinhard, F. G.; Gutiérrez, J.; Morozan, A.; Philouze, C.; Demeshko, S.; Artero, V.; Meyer, F.; de Visser, S. P.; Duboc, C. A Non-Heme Diiron Complex for (Electro)catalytic Reduction of Dioxygen: Tuning the Selectivity through Electron Delivery. *J. Am. Chem. Soc.* **2019**, *141*, 8244−8253.
(55) Monte-Pérez, I.; Kundu, S.; Chandra, A.; Craigo, K. E.; Chernev, P.; Kuhlmann, U.; Dau, H.; Hildebrandt, P.; Greco, C.; Van Stappen, C.; Lehnert, N.; Ray, K. Temperature Dependence of the Catalytic Two- versus Four-Electron Reduction of Dioxygen by a Hexanuclear Cobalt Complex. *J. Am. Chem. Soc.* **2017**, *139*, 15033−15042.
(56) Collman, J. P.; Denisevich, P.; Konai, Y.; Marrocco, M.; Koval, C.; Anson, F. C. Electrode catalysis of the four-electron reduction of oxygen to water by dicobalt face-to-face porphyrins. *J. Am. Chem. Soc.* **1980**, *102*, 6027−6036.
(57) Anson, C. W.; Stahl, S. S. Cooperative Electrocatalytic O_2 Reduction Involving Co(salophen) with *p*-Hydroquinone as an Electron−Proton Transfer Mediator. *J. Am. Chem. Soc.* **2017**, *139*, 18472−18475.
(58) Anson, C. W.; Ghosh, S.; Hammes-Schiffer, S.; Stahl, S. S. Co(salophen)-Catalyzed Aerobic Oxidation of p-Hydroquinone: Mechanism and Implications for Aerobic Oxidation Catalysis. *J. Am. Chem. Soc.* **2016**, *138*, 4186−4193.
(59) Miessler, G.; Fischer, P.; Tarr, D. *Inorganic Chemistry*, 5th Edition; Pearson Education, Inc.: New York, 2014.
(60) Praetorius, J. M.; Allen, D. P.; Wang, R.; Webb, J. D.; Grein, F.; Kennepohl, P.; Crudden, C. M. N-Heterocyclic Carbene Complexes of Rh: Reaction with Dioxygen without Oxidation. *J. Am. Chem. Soc.* **2008**, *130*, 3724−3725.
(61) Frech, C. M.; Shimon, L. J. W.; Milstein, D. Ligand-Controlled Formation of a Low-Valent Pincer Rhodium(I)−Dioxygen Adduct Bearing a Very Short O−O Bond. *Helv. Chim. Acta* **2006**, *89*, 1730−1739.
(62) Hayashi, Y.; Szalda, D. J.; Grills, D. C.; Hanson, J. C.; Huang, K.-W.; Muckerman, J. T.; Fujita, E. Isolation and X-ray structures of four Rh(PCP) complexes including a Rh(I) dioxygen complex with a short O−O bond. *Polyhedron* **2013**, *58*, 106−114.
(63) Busetto, C.; D'Alfonso, A.; Maspero, F.; Perego, G.; Zazzetta, A. Side-on bonded dinitrogen and dioxygen complexes of rhodium(I). Synthesis and crystal structures of trans-chloro(dinitrogen)-, chloro-(dioxygen)-, and chloro(ethylene)-bis(tri-isopropylphosphine)-rhodium(I). *J. Chem. Soc., Dalton Trans.* **1977**, 1828−1834.

https://dx.doi.org/10.1021/acscatal.9b04477
ACS Catal. 2020, 10, 2640−2655

(64) Holland, P. L. Metal-dioxygen and metal-dinitrogen complexes: where are the electrons? *Dalton Trans.* **2010**, *39*, 5415−5425.
(65) Degtyarenko, I.; Nieminen, R. M.; Rovira, C. Structure and Dynamics of Dioxygen Bound to Cobalt and Iron Heme. *Biophys. J.* **2006**, *91*, 2024−2034.
(66) Neese, F. Importance of Direct Spin−Spin Coupling and Spin-Flip Excitations for the Zero-Field Splittings of Transition Metal Complexes: A Case Study. *J. Am. Chem. Soc.* **2006**, *128*, 10213−10222.
(67) Sinnecker, S.; Neese, F. Spin−Spin Contributions to the Zero-Field Splitting Tensor in Organic Triplets, Carbenes and BiradicalsA Density Functional and Ab Initio Study. *J. Phys. Chem. A* **2006**, *110*, 12267−12275.
(68) Huang, X.; Groves, J. T. Oxygen Activation and Radical Transformations in Heme Proteins and Metalloporphyrins. *Chem. Rev.* **2018**, *118*, 2491−2553.
(69) Ali, M. E.; Sanyal, B.; Oppeneer, P. M. Electronic Structure, Spin-States, and Spin-Crossover Reaction of Heme-Related Fe-Porphyrins: A Theoretical Perspective. *J. Phys. Chem. B* **2012**, *116*, 5849−5859.
(70) Wilson, S. A.; Green, E.; Mathews, I. I.; Benfatto, M.; Hodgson, K. O.; Hedman, B.; Sarangi, R. X-ray absorption spectroscopic investigation of the electronic structure differences in solution and crystalline oxyhemoglobin. *Proc. Natl. Acad. Sci. U. S. A.* **2013**, *110*, 16333−16338.
(71) Chen, H.; Ikeda-Saito, M.; Shaik, S. Nature of the Fe−O2 Bonding in Oxy-Myoglobin: Effect of the Protein. *J. Am. Chem. Soc.* **2008**, *130*, 14778−14790.
(72) Singha, A.; Das, P. K.; Dey, A. Resonance Raman Spectroscopy and Density Functional Theory Calculations on Ferrous Porphyrin Dioxygen Adducts with Different Axial Ligands: Correlation of Ground State Wave Function and Geometric Parameters with Experimental Vibrational Frequencies. *Inorg. Chem.* **2019**, *58*, 10704−10715.
(73) Neese, F. The ORCA program system. *Wiley Interdisciplinary Reviews: Computational Molecular Science* **2012**, *2*, 73−78.
(74) Vosko, S. H.; Wilk, L.; Nusair, M. Accurate spin-dependent electron liquid correlation energies for local spin density calculations: a critical analysis. *Can. J. Phys.* **1980**, *58*, 1200−1211.
(75) Lee, C.; Yang, W.; Parr, R. G. Development of the Colle-Salvetti correlation-energy formula into a functional of the electron density. *Phys. Rev. B: Condens. Matter Mater. Phys.* **1988**, *37*, 785−789.
(76) Becke, A. D. Density-functional thermochemistry. III. The role of exact exchange. *J. Chem. Phys.* **1993**, *98*, 5648−5652.
(77) Becke, A. D. A new mixing of Hartree−Fock and local density-functional theories. *J. Chem. Phys.* **1993**, *98*, 1372−1377.
(78) Stephens, P. J.; Devlin, F. J.; Chabalowski, C. F.; Frisch, M. J. Ab Initio Calculation of Vibrational Absorption and Circular Dichroism Spectra Using Density Functional Force Fields. *J. Phys. Chem.* **1994**, *98*, 11623−11627.
(79) Schäfer, A.; Horn, H.; Ahlrichs, R. Fully optimized contracted Gaussian basis sets for atoms Li to Kr. *J. Chem. Phys.* **1992**, *97*, 2571−2577.
(80) Weigend, F.; Ahlrichs, R. Balanced basis sets of split valence, triple zeta valence and quadruple zeta valence quality for H to Rn: Design and assessment of accuracy. *Phys. Chem. Chem. Phys.* **2005**, *7*, 3297−3305.
(81) Izsák, R.; Neese, F. An overlap fitted chain of spheres exchange method. *J. Chem. Phys.* **2011**, *135*, 144105.
(82) Grimme, S.; Antony, J.; Ehrlich, S.; Krieg, H. A consistent and accurate ab initio parametrization of density functional dispersion correction (DFT-D) for the 94 elements H-Pu. *J. Chem. Phys.* **2010**, *132*, 154104.
(83) Grimme, S.; Ehrlich, S.; Goerigk, L. Effect of the damping function in dispersion corrected density functional theory. *J. Comput. Chem.* **2011**, *32*, 1456−1465.
(84) Cossi, M.; Rega, N.; Scalmani, G.; Barone, V. Energies, structures, and electronic properties of molecules in solution with the C-PCM solvation model. *J. Comput. Chem.* **2003**, *24*, 669−681.
(85) Winkler, J. R.; Gray, H. B. Electronic Structures of Oxo-Metal Ions. In *Molecular Electronic Structures of Transition Metal Complexes I*; Mingos, D. M. P., Day, P., Dahl, J. P., Eds.; Springer: Berlin, Heidelberg, 2012; pp 17−28.
(86) Phung, Q. M.; Pierloot, K. The dioxygen adducts of iron and manganese porphyrins: electronic structure and binding energy. *Phys. Chem. Chem. Phys.* **2018**, *20*, 17009−17019.
(87) Lieske, L. E.; Hooe, S. L.; Nichols, A. W.; Machan, C. W. Electrocatalytic reduction of dioxygen by Mn(iii) meso-tetra(N-methylpyridinium-4-yl)porphyrin in universal buffer. *Dalton Trans.* **2019**, *48*, 8633−8641.
(88) Wasylenko, D. J.; Rodríguez, C.; Pegis, M. L.; Mayer, J. M. Direct Comparison of Electrochemical and Spectrochemical Kinetics for Catalytic Oxygen Reduction. *J. Am. Chem. Soc.* **2014**, *136*, 12544−12547.
(89) Sengupta, K.; Chatterjee, S.; Dey, A. In Situ Mechanistic Investigation of O2 Reduction by Iron Porphyrin Electrocatalysts Using Surface-Enhanced Resonance Raman Spectroscopy Coupled to Rotating Disk Electrode (SERRS-RDE) Setup. *ACS Catal.* **2016**, *6*, 6838−6852.
(90) Hooe, S. L.; Rheingold, A. L.; Machan, C. W. Electrocatalytic Reduction of Dioxygen to Hydrogen Peroxide by a Molecular Manganese Complex with a Bipyridine-Containing Schiff Base Ligand. *J. Am. Chem. Soc.* **2018**, *140*, 3232−3241.
(91) Hooe, S. L.; Machan, C. W. Dioxygen Reduction to Hydrogen Peroxide by a Molecular Mn Complex: Mechanistic Divergence between Homogeneous and Heterogeneous Reductants. *J. Am. Chem. Soc.* **2019**, *141*, 4379−4387.
(92) Fourmond, V.; Jacques, P. A.; Fontecave, M.; Artero, V. H2 evolution and molecular electrocatalysts: determination of over-potentials and effect of homoconjugation. *Inorg. Chem.* **2010**, *49*, 10338−47.
(93) McCarthy, B. D.; Dempsey, J. L. Decoding Proton-Coupled Electron Transfer with Potential-pKa Diagrams. *Inorg. Chem.* **2017**, *56*, 1225−1231.
(94) Savéant, J.-M.; Costentin, C. *Elements of Molecular and Biomolecular Electrochemistry: An Electrochemical Approach to Electron Transfer Chemistry*; Wiley: Hoboken, NJ, 2019.
(95) Weschler, C. J.; Hoffman, B. M.; Basolo, F. Synthetic oxygen carrier. Dioxygen adduct of a manganese porphyrin. *J. Am. Chem. Soc.* **1975**, *97*, 5278−5280.
(96) Hoffman, B. M.; Szymanski, T.; Brown, T. G.; Basolo, F. The dioxygen adducts of several manganese(II) porphyrins. Electron paramagnetic resonance studies. *J. Am. Chem. Soc.* **1978**, *100*, 7253−7259.
(97) Jones, R. D.; Summerville, D. A.; Basolo, F. Manganese(II) porphyrin oxygen carriers. Equilibrium constants for the reaction of dioxygen with para-substituted meso-tetraphenylporphinato-manganese(II) complexes. *J. Am. Chem. Soc.* **1978**, *100*, 4416−4424.
(98) Urban, M. W.; Nakamoto, K.; Basolo, F. Infrared spectra of molecular oxygen adducts of (tetraphenylporphyrinato)manganese(II) in argon matrixes. *Inorg. Chem.* **1982**, *21*, 3406−3408.
(99) Wang, Y.-H.; Schneider, P. E.; Goldsmith, Z. K.; Mondal, B.; Hammes-Schiffer, S.; Stahl, S. S. Brønsted Acid Scaling Relationships Enable Control Over Product Selectivity from O2 Reduction with a Mononuclear Cobalt Porphyrin Catalyst. *ACS Cent. Sci.* **2019**, *5*, 1024−1034.
(100) Rosenthal, J.; Nocera, D. G. Oxygen Activation Chemistry of Pacman and Hangman Porphyrin Architectures Based on Xanthene and Dibenzofuran Spacers. In *Progress in Inorganic Chemistry*, Vol. *55*; Karlin, K. D., Ed.; Wiley: Hoboken, NJ, 2008; pp 483−544.
(101) Rakowski Dubois, M.; Dubois, D. L. Development of Molecular Electrocatalysts for CO_2 Reduction and H_2 Production/Oxidation. *Acc. Chem. Res.* **2009**, *42*, 1974−1982.
(102) Nichols, A. W.; Machan, C. W. Secondary-Sphere Effects in Molecular Electrocatalytic CO_2 Reduction. *Front. Chem.* **2019**, *7*, 7.
(103) Bhunia, S.; Rana, A.; Roy, P.; Martin, D. J.; Pegis, M. L.; Roy, B.; Dey, A. Rational Design of Mononuclear Iron Porphyrins for Facile and Selective $4e^-/4H^+$ O_2 Reduction: Activation of O−O Bond by 2nd Sphere Hydrogen Bonding. *J. Am. Chem. Soc.* **2018**, *140*, 9444−9457.

https://dx.doi.org/10.1021/acscatal.9b04477
ACS Catal. 2020, 10, 2640−2655

(104) Savéant, J.-M. Proton Relays in Molecular Catalysis of Electrochemical Reactions: Origin and Limitations of the Boosting Effect. *Angew. Chem., Int. Ed.* **2019**, *58*, 2125−2128.
(105) Fukuzumi, S.; Mandal, S.; Mase, K.; Ohkubo, K.; Park, H.; Benet-Buchholz, J.; Nam, W.; Llobet, A. Catalytic Four-Electron Reduction of O_2 via Rate-Determining Proton-Coupled Electron Transfer to a Dinuclear Cobalt-μ-1,2-peroxo Complex. *J. Am. Chem. Soc.* **2012**, *134*, 9906−9909.
(106) Tse, E. C. M.; Schilter, D.; Gray, D. L.; Rauchfuss, T. B.; Gewirth, A. A. Multicopper Models for the Laccase Active Site: Effect of Nuclearity on Electrocatalytic Oxygen Reduction. *Inorg. Chem.* **2014**, *53*, 8505−8516.
(107) Kataoka, K.; Komori, H.; Ueki, Y.; Konno, Y.; Kamitaka, Y.; Kurose, S.; Tsujimura, S.; Higuchi, Y.; Kano, K.; Seo, D.; Sakurai, T. Structure and Function of the Engineered Multicopper Oxidase CueO from *Escherichia coli*—Deletion of the Methionine-Rich Helical Region Covering the Substrate-Binding Site. *J. Mol. Biol.* **2007**, *373*, 141−152.
(108) Wang, Y.-H.; Pegis, M. L.; Mayer, J. M.; Stahl, S. S. Molecular Cobalt Catalysts for O_2 Reduction: Low-Overpotential Production of H_2O_2 and Comparison with Iron-Based Catalysts. *J. Am. Chem. Soc.* **2017**, *139*, 16458−16461.
(109) Sinha, S.; Ghosh, M.; Warren, J. J. Changing the Selectivity of O_2 Reduction Catalysis with One Ligand Heteroatom. *ACS Catal.* **2019**, *9*, 2685−2691.
(110) Kadish, K. M.; Frémond, L.; Burdet, F.; Barbe, J.-M.; Gros, C. P.; Guilard, R. Cobalt(IV) corroles as catalysts for the electroreduction of O_2: Reactions of heterobimetallic dyads containing a face-to-face linked Fe(III) or Mn(III) porphyrin. *J. Inorg. Biochem.* **2006**, *100*, 858−868.
(111) Askarizadeh, E.; Yaghoob, S. B.; Boghaei, D. M.; Slawin, A. M. Z.; Love, J. B. Tailoring dicobalt Pacman complexes of Schiff-base calixpyrroles towards dioxygen reduction catalysis. *Chem. Commun.* **2010**, *46*, 710−712.
(112) Kolthoff, I. M.; Chantooni, M. K.; Bhowmik, S. Acid-base indicator constants in acetonitrile. *Anal. Chem.* **1967**, *39*, 315−320.
(113) McCarthy, B. D.; Martin, D. J.; Rountree, E. S.; Ullman, A. C.; Dempsey, J. L. Electrochemical Reduction of Brønsted Acids by Glassy Carbon in Acetonitrile—Implications for Electrocatalytic Hydrogen Evolution. *Inorg. Chem.* **2014**, *53*, 8350−8361.
(114) Kütt, A.; Movchun, V.; Rodima, T.; Dansauer, T.; Rusanov, E. B.; Leito, I.; Kaljurand, I.; Koppel, J.; Pihl, V.; Koppel, I.; Ovsjannikov, G.; Toom, L.; Mishima, M.; Medebielle, M.; Lork, E.; Röschenthaler, G.-V.; Koppel, I. A.; Kolomeitsev, A. A. Pentakis(trifluoromethyl)-phenyl, a Sterically Crowded and Electron-withdrawing Group: Synthesis and Acidity of Pentakis(trifluoromethyl)benzene, -toluene, -phenol, and -aniline. *J. Org. Chem.* **2008**, *73*, 2607−2620.
(115) Izutsu, K. (International Union of Pure and Applied Chemistry, Analytical Chemistry Division, Commission on Electroanalytical Chemistry). *Acid-Base Dissociation Constants in Dipolar Aprotic Solvents*; Chemical Data Series, No. *35*; Blackwell Scientific Publications: Oxford, U.K., 1990.
(116) Nielsen, M. F.; Hammerich, O.; Rise, F.; Gogoll, A.; Undheim, K.; Wang, D.-N.; Christensen, S. B. The Effect of Hydrogen Bonding between Methyl-Substituted Phenols and Dipolar Aprotic Solvents on the Rate Constants for Protonation of Anthracene Anion Radical. *Acta Chem. Scand.* **1992**, *46*, 883−896.
(117) Andrieux, C. P.; Hapiot, P.; Saveant, J. M. Mechanism of superoxide ion disproportionation in aprotic solvents. *J. Am. Chem. Soc.* **1987**, *109*, 3768−3775.
(118) Lang, P.; Schwalbe, M. Pacman Compounds: From Energy Transfer to Cooperative. *Chem. - Eur. J.* **2017**, *23*, 17398−17412.
(119) Chang, C. J.; Loh, Z.-H.; Shi, C.; Anson, F. C.; Nocera, D. G. Targeted Proton Delivery in the Catalyzed Reduction of Oxygen to Water by Bimetallic Pacman Porphyrins. *J. Am. Chem. Soc.* **2004**, *126*, 10013−10020.
(120) Chang, C. J.; Deng, Y.; Shi, C.; Chang, C. K.; Anson, F. C.; Nocera, D. G. Electrocatalytic four-electron reduction of oxygen to water by a highly flexible cofacial cobalt bisporphyrin. *Chem. Commun.* **2000**, 1355−1356.
(121) Kakuda, S.; Peterson, R. L.; Ohkubo, K.; Karlin, K. D.; Fukuzumi, S. Enhanced Catalytic Four-Electron Dioxygen (O2) and Two-Electron Hydrogen Peroxide (H2O2) Reduction with a Copper(II) Complex Possessing a Pendant Ligand Pivalamido Group. *J. Am. Chem. Soc.* **2013**, *135*, 6513−6522.
(122) Chatterjee, S.; Sengupta, K.; Hematian, S.; Karlin, K. D.; Dey, A. Electrocatalytic O_2-Reduction by Synthetic Cytochrome c Oxidase Mimics: Identification of a "Bridging Peroxo" Intermediate Involved in Facile $4e^-/4H^+$ O_2-Reduction. *J. Am. Chem. Soc.* **2015**, *137*, 12897−12905.
(123) Costentin, C.; Dridi, H.; Savéant, J.-M. Molecular Catalysis of O2 Reduction by Iron Porphyrins in Water: Heterogeneous versus Homogeneous Pathways. *J. Am. Chem. Soc.* **2015**, *137*, 13535−13544.
(124) Liu, C.; Lei, H.; Zhang, Z.; Chen, F.; Cao, R. Oxygen reduction catalyzed by a water-soluble binuclear copper(ii) complex from a neutral aqueous solution. *Chem. Commun.* **2017**, *53*, 3189−3192.
(125) Machan, C. W. Recent advances in spectroelectrochemistry related to molecular catalytic processes. *Current Opinion in Electrochemistry* **2019**, *15*, 42−49.
(126) Letts, J. A.; Sazanov, L. A. Clarifying the supercomplex: the higher-order organization of the mitochondrial electron transport chain. *Nat. Struct. Mol. Biol.* **2017**, *24*, 800.
(127) Piera, J.; Bäckvall, J.-E. Catalytic Oxidation of Organic Substrates by Molecular Oxygen and Hydrogen Peroxide by Multistep Electron Transfer—A Biomimetic Approach. *Angew. Chem., Int. Ed.* **2008**, *47*, 3506−3523.
(128) Baeckvall, J.-E.; Hopkins, R. B.; Grennberg, H.; Mader, M.; Awasthi, A. K. Multistep electron transfer in palladium-catalyzed aerobic oxidations via a metal macrocycle quinone system. *J. Am. Chem. Soc.* **1990**, *112*, 5160−5166.
(129) Bäckvall, J.-E.; Chowdhury, R. L.; Karlsson, U. Ruthenium-catalysed aerobic oxidation of alcohols via multistep electron transfer. *J. Chem. Soc., Chem. Commun.* **1991**, 473−475.
(130) Pegis, M. L.; Wise, C. F.; Koronkiewicz, B.; Mayer, J. M. Identifying and Breaking Scaling Relations in Molecular Catalysis of Electrochemical Reactions. *J. Am. Chem. Soc.* **2017**, *139*, 11000−11003.
(131) Costentin, C.; Savéant, J.-M. Homogeneous Molecular Catalysis of Electrochemical Reactions: Manipulating Intrinsic and Operational Factors for Catalyst Improvement. *J. Am. Chem. Soc.* **2018**, *140*, 16669−16675.
(132) Machan, C. W.; Chabolla, S. A.; Yin, J.; Gilson, M. K.; Tezcan, F. A.; Kubiak, C. P. Supramolecular Assembly Promotes the Electrocatalytic Reduction of Carbon Dioxide by Re(I) Bipyridine Catalysts at a Lower Overpotential. *J. Am. Chem. Soc.* **2014**, *136*, 14598−14607.
(133) Machan, C. W.; Yin, J.; Chabolla, S. A.; Gilson, M. K.; Kubiak, C. P. Improving the Efficiency and Activity of Electrocatalysts for the Reduction of CO2 through Supramolecular Assembly with Amino Acid-Modified Ligands. *J. Am. Chem. Soc.* **2016**, *138*, 8184−93.
(134) Machan, C. W.; Kubiak, C. P. Interrogating heterobimetallic co-catalytic responses for the electrocatalytic reduction of CO2 using supramolecular assembly. *Dalton Transactions* **2016**, *45*, 15942−15950.
(135) Chabolla, S. A.; Machan, C. W.; Yin, J.; Dellamary, E. A.; Sahu, S.; Gianneschi, N. C.; Gilson, M. K.; Tezcan, F. A.; Kubiak, C. P. Bio-inspired CO2 reduction by a rhenium tricarbonyl bipyridine-based catalyst appended to amino acids and peptidic platforms: incorporating proton relays and hydrogen-bonding functional groups. *Faraday Discuss.* **2017**, *198*, 279−300.
(136) Sahu, S.; Cheung, P. L.; Machan, C. W.; Chabolla, S. A.; Kubiak, C. P.; Gianneschi, N. C. Charged Macromolecular Rhenium Bipyridine Catalysts with Tunable CO2 Reduction Potentials. *Chem. - Eur. J.* **2017**, *23*, 8619−8622.
(137) Borovik, A. S. Bioinspired Hydrogen Bond Motifs in Ligand Design: The Role of Noncovalent Interactions in Metal Ion Mediated Activation of Dioxygen. *Acc. Chem. Res.* **2005**, *38*, 54−61.
(138) Shook, R. L.; Borovik, A. S. The effects of hydrogen bonds on metal-mediated O2activation and related processes. *Chem. Commun.* **2008**, 6095−6107.
(139) Guo, M.; Lee, Y.-M.; Gupta, R.; Seo, M. S.; Ohta, T.; Wang, H.-H.; Liu, H.-Y.; Dhuri, S. N.; Sarangi, R.; Fukuzumi, S.; Nam, W.

https://dx.doi.org/10.1021/acscatal.9b04477
ACS Catal. 2020, 10, 2640−2655

Dioxygen Activation and O−O Bond Formation Reactions by Manganese Corroles. *J. Am. Chem. Soc.* **2017**, *139*, 15858−15867.
(140) Jung, J.; Liu, S.; Ohkubo, K.; Abu-Omar, M. M.; Fukuzumi, S. Catalytic Two-Electron Reduction of Dioxygen by Ferrocene Derivatives with Manganese(V) Corroles. *Inorg. Chem.* **2015**, *54*, 4285−4291.
(141) Mase, K.; Ohkubo, K.; Fukuzumi, S. Much Enhanced Catalytic Reactivity of Cobalt Chlorin Derivatives on Two-Electron Reduction of Dioxygen to Produce Hydrogen Peroxide. *Inorg. Chem.* **2015**, *54*, 1808−1815.
(142) Blakely, M. N.; Dedushko, M. A.; Yan Poon, P. C.; Villar-Acevedo, G.; Kovacs, J. A. Formation of a Reactive, Alkyl Thiolate-Ligated FeIII-Superoxo Intermediate Derived from Dioxygen. *J. Am. Chem. Soc.* **2019**, *141*, 1867−1870.
(143) Yan Poon, P. C.; Dedushko, M. A.; Sun, X.; Yang, G.; Toledo, S.; Hayes, E. C.; Johansen, A.; Piquette, M. C.; Rees, J. A.; Stoll, S.; Rybak-Akimova, E.; Kovacs, J. A. How Metal Ion Lewis Acidity and Steric Properties Influence the Barrier to Dioxygen Binding, Peroxo O−O Bond Cleavage, and Reactivity. *J. Am. Chem. Soc.* **2019**, *141*, 15046−15057.
(144) Creager, S. E.; Raybuck, S. A.; Murray, R. W. An efficient electrocatalytic model cytochrome P-450 epoxidation cycle. *J. Am. Chem. Soc.* **1986**, *108*, 4225−4227.
(145) Horwitz, C. P.; Creager, S. E.; Murray, R. W. Electrocatalytic olefin epoxidation using manganese Schiff-base complexes and dioxygen. *Inorg. Chem.* **1990**, *29*, 1006−1011.
(146) Zidane, Y.; Ourari, A.; Bataille, T.; Hapiot, P.; Hauchard, D. Electrochemical study with cavity microelectrode containing clay-supported Mn(III)salen complex − Dioxygen activation with cytochrome P450 model. *J. Electroanal. Chem.* **2010**, *641*, 64−70.
(147) Natinsky, B. S.; Lu, S.; Copeland, E. D.; Quintana, J. C.; Liu, C. Solution Catalytic Cycle of Incompatible Steps for Ambient Air Oxidation of Methane to Methanol. *ACS Cent. Sci.* **2019**, *5*, 1584−1590.
(148) Pettersen, E. F.; Goddard, T. D.; Huang, C. C.; Couch, G. S.; Greenblatt, D. M.; Meng, E. C.; Ferrin, T. E. UCSF Chimera—A visualization system for exploratory research and analysis. *J. Comput. Chem.* **2004**, *25*, 1605−1612.
(149) Connelly, N. G.; Geiger, W. E. Chemical Redox Agents for Organometallic Chemistry. *Chem. Rev.* **1996**, *96*, 877−910.
(150) Pavlishchuk, V. V.; Addison, A. W. Conversion constants for redox potentials measured versus different reference electrodes in acetonitrile solutions at 25°C. *Inorg. Chim. Acta* **2000**, *298*, 97−102.
(151) Sawyer, D. T.; Sobkowiak, A.; Roberts, J. L. *Electrochemistry for Chemists*, 2nd Edition; John Wiley & Sons, Inc.: New York, 1995.

https://dx.doi.org/10.1021/acscatal.9b04477
ACS Catal. 2020, 10, 2640−2655